ABSTRACT

Title of Document: INTERFERENCE STUDIES USING MULTIDIMENSIONAL MAPPING OF CROSS-REACTIVE SENSORS: APPLICATIONS IN BLOOD MONITORING OF CLOZAPINE

Sheryl E. Chocron, Master of Science, 2014

Directed By: Reza Ghodssi, Herbert Rabin Distinguished Chair of Engineering, Electrical and Computer Engineering

Point-of-care sensors are used in clinical applications for diagnosing and monitoring health conditions. For example, a point-of-care sensor for therapeutic drug monitoring of the clozapine antipsychotic can reduce burdens from guidelines suggesting routine monitoring of this medication. However, when measuring chemical markers in complex fluids, there are challenges related to decreased sensor performance due to chemical interference. This work presents a methodology for identifying individual interfering species. A set of cross-reactive electrochemical sensors were developed, whose diversified responses provide a fingerprint-type pattern capable of differentiating various species. By mapping the multidimensional responses, patterns from complex solutions were discerned and matched to those of individual species. Applying this methodology to clozapine sensing in blood, a major source of chemical interference was identified. The understanding matrix components that cause interference can guide the design of reliable sensing systems and can be integrated with pattern recognition tools that can account for it.

INTERFERENCE STUDIES USING MULTIDIMENSIONAL MAPPING OF CROSS-REACTIVE SENSORS: APPLICATIONS IN BLOOD MONITORING OF CLOZAPINE

By

Sheryl E. Chocron

Thesis submitted to the Faculty of the Graduate School of the
University of Maryland, College Park, in partial fulfillment
of the requirements for the degree of
Master of Science
2014

Advisory Committee:
Reza Ghodssi, Chair
Deanna L. Kelly
Gregory F. Payne
Ian M. White

Acknowledgements

First, I would like to thank my advisor, Dr. Reza Ghodssi, and the rest of my committee members: Dr. Deanna L. Kelly, Dr. Gregory F. Payne and Dr. Ian M. White. I thank all the members of the MEMS Sensors and Actuators Laboratory (MSAL), especially Dr. Hadar Ben-Yoav, Thomas Winkler, and Dr. Konstantinos Gerasopoulos for their support and guidance. I would also like to thank two outstanding undergraduate students that I had the pleasure to work directly with, Bryce Weisberger and Michelle Patkin.

I acknowledge the Robert W. Deutsch Foundation and the Maryland Innovation Initiative for funding this work, and the National Science Foundation for awarding me the Graduate Research Fellowship. I also thank our collaborators Dr. Deanna L Kelly, Dr. Gregory F. Payne, Dr. Eunkyoung Kim, and the Biochip Collaborative members for their teamwork and support.

Finally, I thank my husband Frederic Spieler as well as my parents and siblings, who encouraged and guided me.

Table of Contents

List of Tables

List of Figures

Chapter 1: Introduction

1.1 Motivation and Objectives

The motivation behind this work lies in the need for methods and guidance in relation to the design of sensors for testing complex solutions, where a large number of unknown and potentially interfering species are present. When measuring chemical information in biological fluids, challenges of interference from other species in the solution arise, especially in sensing applications where no biological recognition elements exist. An understanding of the species in these complex matrices that affect a particular sensor system is useful in guiding its design.

This thesis demonstrates a study of interfering species for the application of real-time therapeutic drug monitoring (TDM), which is used to monitor the efficacy and safety of drug treatments. The antipsychotic clozapine (CLZ) is a fitting example of the need of frequent TDM in schizophrenia. It is the most effective antipsychotic for treatment-resistant schizophrenia and because of its narrow therapeutic range frequent measurement of CLZ blood level is recommended [1]. CLZ is currently routinely measured by trained professionals at centralized laboratory facilities [2]. However, the iterative nature of this practice creates a burden for patients and medical professionals. Thus, a faster and more convenient POC monitoring platform that can be employed on-site or at home has the potential to decrease the burden and improve treatment outcomes. The methodology and tools presented in this thesis specifically

addresses selectivity issues that arise from interfering species present in blood serum samples with regard to CLZ blood monitoring.

The objective of this thesis is to demonstrate a methodology for characterizing interfering species in electrochemical sensors, validated in the application of CLZ antipsychotic TDM in blood serum. The methodology, illustrated in Figure 1, begins with a coarse screening of interfering species relevant to CLZ sensing and proceeds with increased characterization rigor as the interfering species are narrowed down. The next stage of this methodology uses cross-reactive sensors to discern and match multidimensional patterns across buffer and complex fluid sample matrices. By matching the buffer and complex fluid responses, individual interfering species present in complex matrices (*i.e.*, serum is composed of hundreds of species) can be identified. A feedback loop allows for various iterations of screening and matching. This multi-level test provides patterns that can be classified to particular species of interest. The results will help guide more targeted sensor design as well as future integration with sensor array pattern analysis tools, such as chemometric models.

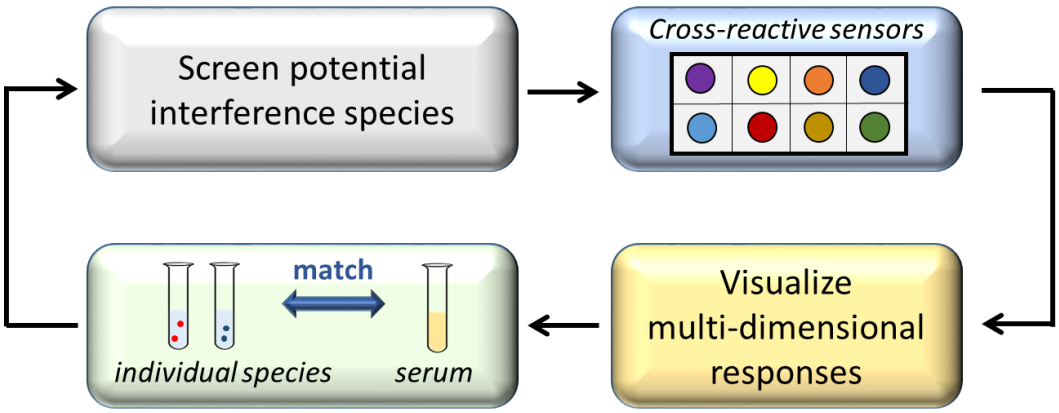

Figure 1. Schematic representing the systematic methodology for studying the effect of the presence of interfering species (IS) presence on the CLZ measurement by matching buffer-based and serum studies through the use of cross-reactive sensors (CRS). A feedback loop enables various iterations of screening and matching of interfering species to narrow down all the major species.

1.2 Background

In this section, the context of the thesis research is established. The main POC sensing paradigms and current challenges regarding sample interference in complex matrices are reviewed. The concept of TDM as it relates to CLZ management is introduced. Lastly, the sensing methods of this study (electrochemical sensing and sensor arrays) are discussed.

1.2.1 Point-of-Care Sensors for Blood Analysis

1.2.1.1 Overview

Point-of-Care (POC) sensors for blood analysis, such as in vitro diagnostics (IVD), are real-time devices used to maintain health, manage disease or monitor therapy and are decentralized, meaning that they can be carried out without the need for laboratory professionals and central facilities [3]. Rather, they are employed either in a near-patient setting (*i.e.*, clinic, doctor's office, pharmacy) or at home (*i.e.*, glucometers, pregnancy tests). The advantages of POC technologies include faster results and therapeutic interventions, improved patient compliance, decreased hospital visits, better quality of life, and reduced cost [3-5]. The devices are designed to test one or multiple blood components such as proteins, nucleic acids, metabolites, drugs, dissolved gases, cells, and ions in biological fluids (*i.e.*, blood, saliva, urine) [3]. Ideal POC devices contain inexpensive platforms (*i.e.*, disposable cartridges) that include microfluidic flow control, sensor elements, and readout capabilities. The focus of this thesis will be on the sensor element.

The general lock-and-key design of sensor elements for measurement of biological analytes consists of a recognition element and a transducer, which is coupled to a signal readout [6, 7]. The recognition element is a component that interacts (*i.e.*, binds or recognizes) with the analyte, imparting selectivity for the analyte in the presence of other species in complex biological fluids. Some examples of recognition elements commonly used in blood analysis include enzymes, antibodies and proteins. The transducer is a detector element that transforms the signal resulting from the interaction of the analyte with the recognition element into a signal that is measurable. Examples of common transducers include optical, piezoelectric, and electrochemical sensing methods [7]. The optimal choice of recognition and transducer elements should correspond to acceptable selectivity and sensitivity requirements depending on the application [8]. For instance, the physiological range of analyte concentrations, sample processing and component stability limitations, desired sensing time, and interference from sample components are some of the considerations for selecting an appropriate combination of elements for the sensor design [3, 6-8].

Two of the most well-known and successful POC tests include the blood glucose and pregnancy tests [3, 5]. Glucose sensors account for over 85% of the biosensors market [9], and they are used for diabetes monitoring. The concept of glucose monitoring is straightforward; people with diabetes test their glucose levels a few times a day, which helps them assess whether an insulin dose is needed at the particular time of day and helps to evaluate the success of diet and exercise. Glucose sensors are typically composed of enzymatic elements (glucose oxidase) assembled onto

electrochemical sensors. The glucose molecules are recognized by the enzyme, which also serves as a transduction element since it is coupled to a secondary reaction. The product of the second reaction is electrochemically detected and serves as an indirect measurement of the glucose concentration.

The most common paradigm for biological sensor designs is the glucometer; thus, its design is typically used for sensing of a variety of other analytes. However, in cases where no specific recognition element is known for an analyte, a modified approach that is commonly employed is the use of indirect or synthetic recognition elements. These elements consist of sensitive coating materials that exhibit preferential properties for the analyte, and they are further discussed in section 1.2.3.2.

1.2.1.2 Interference Challenges

Interference is defined as a cause of significant bias in the analyte measurement due to the effect of another component or property of the sample [10]. Interferences in complex biologic matrix is a particular challenge of biological sensors [11, 12]. Some of the major modes of interference from species in a complex sample are illustrated in Figure 2. Direct detection of matrix components at the sensor surface is a major type of interference that can lead to chemical artifacts to ultimately project false positive results. Sensors with non-specific or no recognition elements are particularly susceptible to this type of interference and they are likely to suffer from a wider pool for interfering species due to the lack of selectivity. Deposition of species on the electrode surface (fouling) is another major type of interference whose major result is

a decrease in sensor sensitivity and functionality. Lastly, species in the sample may react with each other prior to measurement due depending on storage and handling conditions and stability of the species.

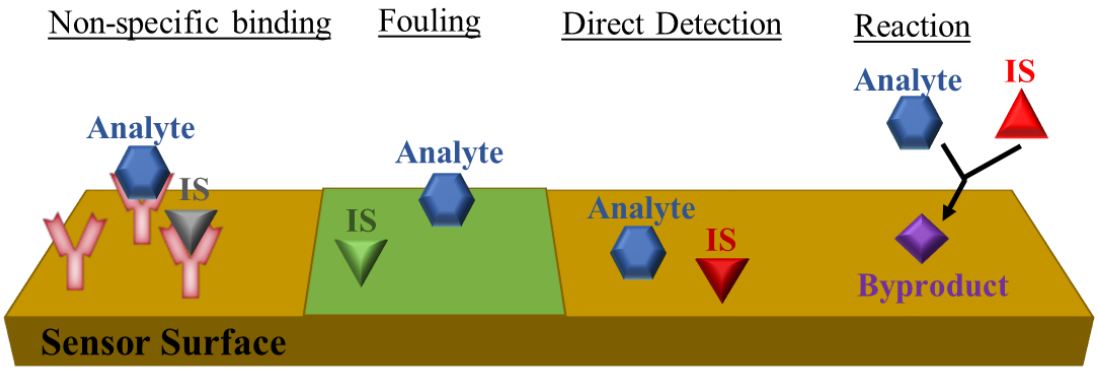

Figure 2. Illustration of four major modes of interference for the measurement of the analyte from interfering species (IS) in complex smaples: non-specific binding to recognition elements, fouling of the sensor surface, direct detection, and reaction between sample components prior to measurement.

Potentially interfering species encompass endogenous species (*i.e.*, naturally present in samples matrix) and exogenous species (*i.e.*, originating outside the body). In serum, hundreds of endogenous species are present pertaining to the following classes: vitamins, minerals, amino acids, sugars, lipids, and proteins. Ascorbic acid, uric acid, oxygen and proteins are common endogenous interfering species [13-15]. Exogenous species include medications, ingested substances, and substances added during sample preparation [10]. Acetaminophen, maltose, salicylic acid, and xanthine are common exogenous interfering species [9, 13, 15, 16]. The concentration of both endogenous and exogenous species varies across the population, and thus the interference is variable from one individual to another. For this reason, understanding

the source of interferences can aid in accounting for interferent-specific effects on the sensor measurement.

Some approaches that can be used to account for interfering species include chemical treatment, separation techniques (*i.e.*, chromatography, extraction, filtration), manipulating molecular interactions at the sensor surface (*i.e.*, size exclusion, electrostatic forces, catalytic behavior) or applying signal processing methods (*i.e.*, deconvolution, noise filters, chemometrics). The first two methods involve the removal of the interfering species of interest, which are most common in clinical laboratories because they ensure elimination of the sensor interference. However, this may be difficult to integrate into POC sensors because specialized equipment and personnel are typically required, and separation may affect other properties (including the analyte) of the sample. For these practical reasons, employment of materials at the sensor surface to manipulate molecular interactions is a more typical approach in the design of POC sensors. This approach imparts some level of selectivity to the sensor, and these types of sensors are referred to as semi-selective in contrast to selective sensors which contain recognition elements with high levels of selectivity. Nonetheless, this approach suffers because molecular interactions can affect a variety of sample components as well as the analyte. For example, using a material coating that attracts the positive charge of an analyte will presumably repel negatively charged species, however, it will also attract other positively charged species in the complex sample. Due to the large number of species present in complex samples, it can be difficult to exclude all but one type of species with a single sensor. Lastly,

while the signal processing approach does not affect the sample since it is an end-point technique, it may require a large number of samples and it has the potential to introduce computational artifacts. In all the cases, knowledge of the major interfering species affecting a particular sensor enables the design of a targeted approach to reduce the effect of those species. Without this knowledge or if only general information is known (*i.e.*, the species known to interfere in other sensors), trial and error methods and preliminary assumptions must be employed. The latter is time consuming and has the potential for missing interfering species that are particular for the individual sensor.

1.2.2 Therapeutic Drug Monitoring: Clozapine

TDM refers to the quantification of serum or plasma concentrations of medications for use in dose optimization and tailoring [17, 18]. Measurement of drug concentration has only been proven helpful in circumstances where drug adherence is uncertain, there is a narrow therapeutic range, there is no response of therapeutic dosage, or pharmacokinetic drug-drug interaction is typical [2, 17]. TDM is based on the assumption that plasma concentrations correlates to clinical effects and has a therapeutic window of maximal safety and efficacy. The lower therapeutic limit corresponds to the concentration under which therapeutic response is unlikely, and the upper therapeutic limit refers to the concentration above which tolerability decreases.

In psychiatry, TDM can be useful due to the variability in inter-individual treatment response. The 2011 published guidelines for TDM in psychiatry rated 128 neuropsychiatric drugs according to the usefulness and recommendation for TDM [17]. According to these guidelines, TDM is especially necessary for drugs with narrow therapeutic ranges, where close monitoring can guide drug titration after the initial prescription of after dose changes. Currently, TDM has become routine for a considerable number of psychopharmacologic compounds with clear evidence of its benefits. For instance, TDM has become the standard of care for lithium as well as CLZ treatment due to their narrow therapeutic range. However, regular monitoring of these medications can be burdensome for patients and doctors. For this reason, technologies capable of monitoring therapeutic concentrations of these medications in real-time and at the POC would aid in treatment management.

Lithium and CLZ are important neuropsychiatric medications because they are effective for treatment resistant unipolar depression and schizophrenia, respectively. Lithium is a mood stabilizer with a therapeutic range of 4 – 8 μg/mL (0.4 – 1.2 mM). FDA-approved POC devices for lithium TDM exist in the commercial sector, such as the colorimetric ReliaLAB instrument. This instrument consists of a blood separator membrane to separate plasma from blood, which is added to a prefilled cuvette containing a colorimetric agent and placed in a photometric reader [19]. Clozapine (CLZ) is the most effective antipsychotic treatment-resistant schizophrenia with a therapeutic range of 0.35 – 1 μg/mL (1 – 3 μM) [2, 17, 20]. CLZ blood monitoring, on the other hand, is currently carried out centralized laboratory facilities because no

POC CLZ TDM exists in the market. Our research group at UMD, in a collaborative effort with Dr. Deanna Kelly at the Maryland Psychiatric Research Center (UMB) and Dr. Gregory Payne at UMD, has been working towards developing a POC solution for CLZ TDM using microsystem technology for the past 3 years. Our research aims to monitor the CLZ treatment [21] as well as white blood cells (WBCs) [22], whose measurement is recommended for monitoring agranulocytosis, a primary side effect of CLZ treatment. As shown in Figure 3, the aim is to integrate both monitoring technologies such that a point-of-care solution can be developed, which has the potential to decrease the burden of CLZ treatment monitoring and increase efficacy of this treatment [21-23]. Moreover, these technologies represent model systems for integrate POC diagnostic and prognostic devices.

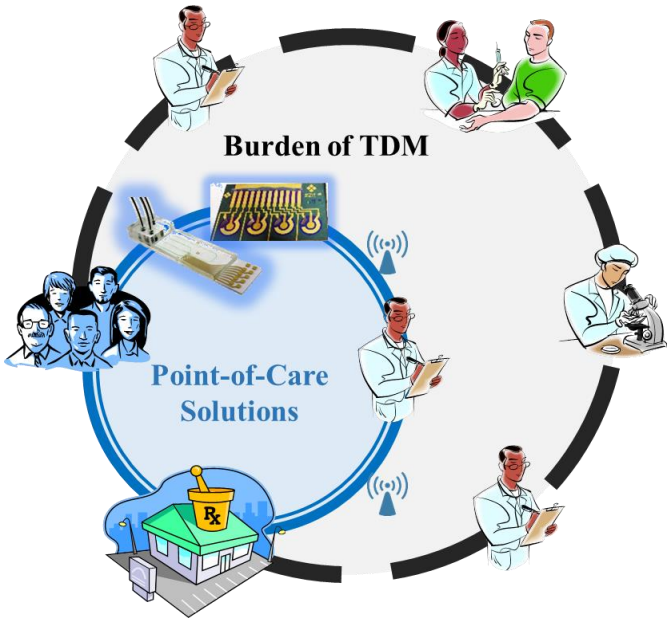

Figure 3. Closing the loop with microsystems technologies. The big loop shows the number of stages and amount of personnel needed for monitoring blood levels in current practice, which represents a burden for the patients and the doctors. The smaller loop represents the convenience of POC solutions (such as the CLZ and the WBC monitors developed in our group [21, 22]), which can decrease the burden and increase the efficiency of CLZ management. These microsystems are amenable to wireless communication, which would further increase the convenience for doctors, pharmacy and patient.

1.2.3 Bioelectrochemical Sensing

1.2.3.1 Overview

Bioelectrochemical methods refer to the measurement of electrical properties of a biological system for extracting information. Electrochemical techniques are rapid and have been successfully applied to trace measurements due to their high sensitivity and selectivity [24]. Analytes in solution can be measured by applying electrical energy (*i.e.*, current or voltage) through electrodes and measuring the electrical response. The three major methods can be divided according to the type of electrical signal that is applied and measured: potentiometry (constant current is applied as the potential is measured), coulometry (constant potential is applies as the current is measured), and voltammetry (altering potential is applied as the current is measured). While potentiometry and coulometry are ideal for systems where interference from other sample components is avoidable, voltammetry can provide additional distinguishing parameters for separating the potential response signals of various species.

Voltammetric responses contain two major components that represent the electroactive species and its concentration: the oxidation or reduction peak potential (E_p) which is a compound-specific value correlating to the ability of a species to donate electrons at a particular energy, and the oxidation or reduction peak current (I_p) which correlates to the species concentration [24]. Thus, voltammetry has a grade of selectivity that depends applied potential range and the number of species that are active in this range [24]. Furthermore, additional peaks or shifts of the main peak can

occur if the reaction proceeds, providing more patterns to differentiate the analyte of interest [24].

Interference and electrode fouling are two major problems of electrochemical sensors [9], as discussed in section 1.2.1.2. For instance, if the applied potential required to oxidize or reduce the analyte of interest can also oxidize other species present in the sample, this will result in a response that overestimates the analyte concentration and cause peak overlap of their individual responses [14].

1.2.3.2 Electrode Materials

Advances in material science and nanotechnology have led to the development of a wide variety of electrode material coatings that serve as highly sensitive and semi-selective materials in a sensor. Carbon based materials have lower background oxidation currents compared to metal electrodes. Carbon nanotubes, for instance, can be coated on electrodes to create high surface areas with fast electron transfer kinetics, which increases the sensitivity and decreases the potential required for redox reactions [25, 26]. The increased resolution of electrochemical peaks can provide the ability to better differentiate current responses of species with similar peak potentials. Similarly, nanoparticle-modified electrodes have been shown to confer catalytic activity and may change electrode kinetics and reaction mechanisms due to the changed electronic structure at the nanoscale [27]. Furthermore, electrodes may be chemically modified via self-assembly monolayers (SAM) or polymer film formation. The use of thiol SAMs on gold electrodes is a well-known example, although

limitations exist with the low-density monolayer coverage this technique can achieve [28]. Electrode modifications involving polymer coatings are also advantageous due to their ability to electrodeposit onto electrode surfaces to form tunable coatings that can be functionalized. For instance, molecularly imprinted polymers (MIPS) are synthetic polymers used to mimic the specific recognition of enzyme elements. MIPS are fabricated by spatially arranging and cross-linking monomers around template molecules, which are then removed such that the final product is able to rebind the original template molecule [29]. MIPS can be used as a recognition element in a biosensor or as a means for extracting low-concentration species. Another class of polymer coating involve conductive polymers, such as polypyrrole and polyaniline, which have low electrical resistivity and amplify electrochemical responses due to their high conductive surface areas [8, 30]. Moreover, in a recent review by our group, the versatility of electrode coatings made with chitosan polymers were shown to be deposited controllably, to direct electrochemistry of proteins, to control permeability, to modify nanostructures, and to act as a graft for other functional molecules [31]. Our collaborators Dr. Eunkyoung Kim and Dr. Gregory Payne demonstrated the electrochemical grafting of catechol moieties onto the chitosan film, creating a redox cycling system (RCS) [32, 33]. By grafting electroactive catechol moieties close to the surface of the electrode, the material coating was shown to reduce species after being oxidized at the electrode such that a cycle of oxidation and reduction is created. In that manner, the RCS can amplify the electrochemical signal of the analyte via redox cycling by increasing the number of electrons transferred at the electrode. Lastly, electrochemical sensors are amenable to miniaturization due to

its synergy with electronics and micro-scale fabrication, where sensing electrodes can be incorporated directly on-chip.

1.2.3.3 Electrochemical Clozapine Detection

CLZ belongs to a large class of drugs structurally defined as dibenzo-1,4-diazepines, which undergo reversible 2 electron/one proton redox reactions [34]. Van Leeuwen et al. showed the following scheme (scheme 1), where CLZ can be semi-reversibly oxidized and reduced. Due to the instability of reaction products, the reversibility is not complete because (electroactive) byproducts form after CLZ oxidation. The major electroactive byproduct is thought to correlate to hydroxylated CLZ derivatives and is also reversible [35]. Figure 4 illustrates the cyclic voltammetry response for clozapine at a carbon paste electrode, where oxidation and reduction peaks are seen for the clozapine redox reaction and similarly for the byproduct redox reaction [36].

(1) $$CLZ \leftrightarrow CLZ^{+1} + 2H^{+1} + 2e^{-1} \rightarrow Byproduct \leftrightarrow Byproduct'$$

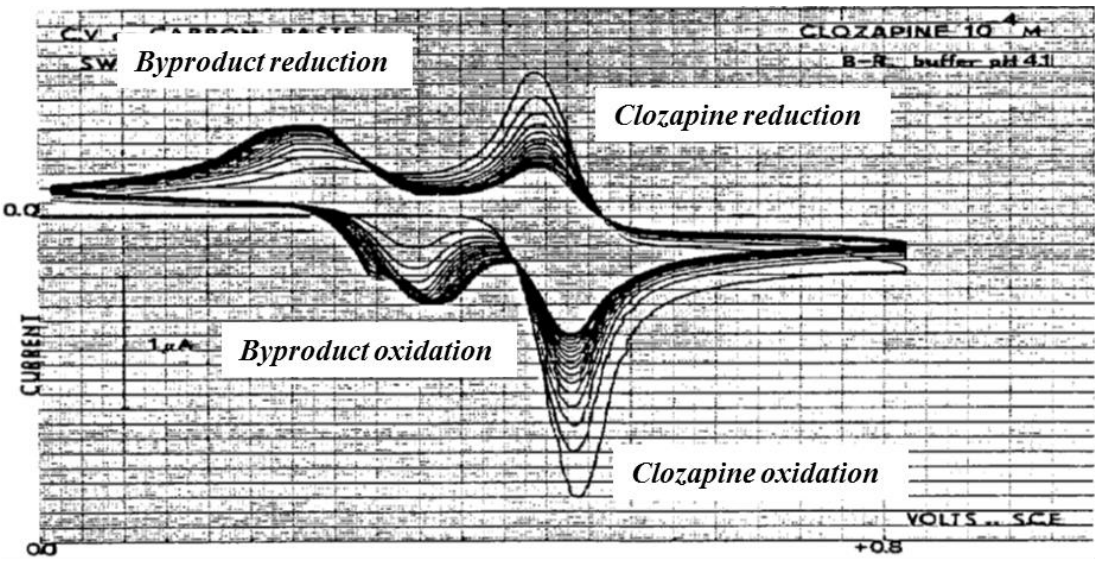

Figure 4. Cyclic voltammetry of clozapine at a carbon paste electrode, illustrating the redox reaction. The larger oxidation and reduction peaks correlate to the primary clozapine reaction, and the smaller oxidation and reduction peaks correlate to the byproduct reaction [36].

Electrochemical CLZ sensing systems have been shown in the literature over the years. A vast majority of them show electrochemical analysis in buffer-based solutions [36-47], with a large subset demonstrating detection of CLZ in pharmaceutical samples for applications in quality control [37-40, 42, 43, 46, 48], and a minority demonstrating detection in human blood serum or plasma samples [37, 39-41, 46]. Recently, our group published results of a micro-scale CLZ sensor based on chitosan-catechol redox cycling system (ccRCS) modified electrodes, in buffer and untreated serum samples [21].

Of those sensors demonstrating detection in human serum or plasma, all contained pre-treatment steps that included diluting, changing the pH, and removing the proteins from the sample. The only exception is our ccRCS based sensor, for which the serum sample was not pre-treated [21]. Yet it demonstrated challenges in the detection of CLZ at the lower end of its therapeutic range [21]. Of those studies that

show the application for serum-based measurements, only a minority carried out an interference study [37, 46]. Additionally, only a few demonstrate the raw electrochemical response of serum-based samples, where it is clear that an oxidative background signal of serum (present even in the treated samples) appears at a location close to that of the CLZ oxidation, and seems to be convoluted with the CLZ peak [21, 40, 41]. Lastly, only a partial study of interfering species has been carried out for CLZ sensors, and the abovementioned background peak has not been assigned to any particular species or effect, to the best of my knowledge. In order to achieve CLZ detection in human serum matrices and translate the sensor design to micro-scale POC devices, a design with minimal pre-treatment steps and sensor modification amenable to microsystem fabrication is strongly preferred. Moreover, an understanding of the background signals of interfering species present in the serum sample matrix can guide a more targeted design for a POC CLZ sensor.

1.2.4 Cross-Reactive Sensor Arrays

Whereas the design of single, highly selective lock-and-key sensors have been used for species with specific recognition elements, a related approach uses a semi-selective, cross-reactive sensor (CRS) that capitalizes on physicochemical effects and molecular interactions to impart some selectivity toward an analyte [49, 50], as mentioned in section 1.3.2.2. The latter approach is appropriate when a specific target compound is measured in controlled backgrounds or when the composition of the fluid matrix is known [49]. Thus, challenges and limitations arise in the case of complex fluids (*i.e.*, blood serum, food and beverages, perfumes) where variable

backgrounds with intricate interactions exist. However, a strategy that addresses this challenge is the employment of CRS arrays, inspired by the biological function of the olfactory system in odor detection [49]. Studies have shown that each individual olfactory receptor is not highly specific but rather each receptor can respond to many analytes and it is the integrated response of a combination of receptors that enables identification of odors [49, 51]. Olfactory receptors are cross-reactive, meaning that they can be activated by a variety of odorants.

The concept of employing CRS arrays for chemical detection was given the term "artificial or electronic noses and tongues" (depending on the phase of the sample) [50-54]. As illustrated in Figure 5, the combination of olfactory receptors activated by the coffee odorant sends a set of signals to the brain, which processes the information and matches it to a database of odors in order to identify the smell. Similarly, the coffee odorant generates a response from a combination of CRS in the artificial nose system, whose signal is processed by a pattern recognition model (*i.e.*, commonly chemometrics) and is compared to a previously obtained database in order to identify the smell. In this way, the artificial nose/tongue concept mimics the processes for sensing in the biological sensory system.

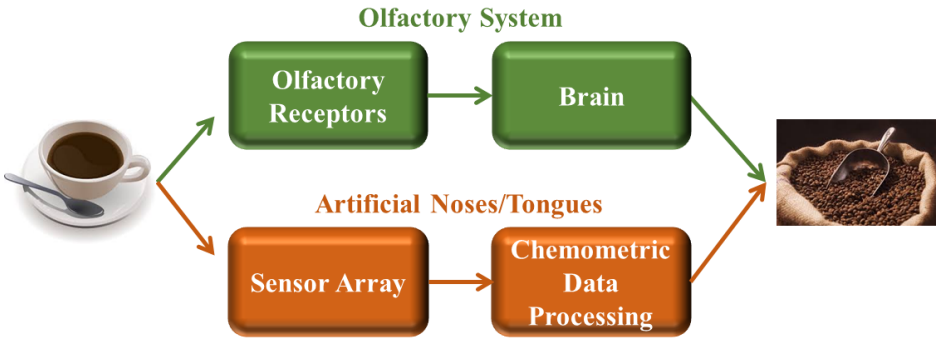

Figure 5. The schematic shows the order of events of how coffee is sensed. The smell of coffee binds to a series of olfactory receptors, which send signals to the brain, which interprets the receptor sequence to interpret the source of the smell. Similarly, the smell of coffee binds differentially to a series of sensors in an array, whose response is analyzed by a chemometric data processing model, which matches the pattern with a database to interpret the odor.

The advantage of utilizing an artificial tongue approach is the ability to yield responses for a variety of analytes, including those for which the sensor was not originally designed to detect. The array integrates the responses of a variety of components of the complex matrix such that a unique pattern for the complex solution is generated without the requirement of prior knowledge of individual components. Such arrays should be designed such that the sensors are cross-reactive to the diversity of analytes and their concentrations in the sample. CRS refer to receptors that are generalized rather than specialized. Thus, receptors need not be designed to target specific analytes but rather need to be designed to be differential, such that added and synergistic patterns are provided by additional sensors in the array [50]. Additionally, CRS should provide diversified responses such that each additional sensor provides additional information. For instance, an additional sensor may be cross-reactive to other components of the sample or may provide an orthogonal measurement of the same compounds. Electrochemical sensors utilized for creating arrays include employing various voltammetric sensing techniques [55-57],

polymeric [54, 56, 58-63] and chemical [64] electrode modifications, or electrode materials [52, 53].

By relying on patterns of the multi-sensor response, the sensor system reduces the need for selectivity [49]. In order to realize the full-potential of CRS arrays, signal processing methods are employed to integrate the multivariate response patterns across the array. Common signal processing algorithms used in artificial tongues are chemometric techniques, which are numerical techniques that extract useful information from chemical systems [65]. Quantitative or qualitative models can be applied to obtain either presence/absence information or concentration values [66]. Moreover, advanced models such as artificial neural networks are capable of being trained to a certain sample matrix, such as the particular baseline signal of an individual's serum, and can account for the sample matrix changes that may differ from person to person [67]. Thus, the diversity of a sensor array provides multidimensional information that can account for variable interfering species in blood. One can account for known interferents within the algorithm, and some papers have gone as far as to show how they are capable of de-convoluting conflicting response peaks [68-70]. Common chemometric algorithms include principal component analysis (PCA), partial least squares regression (PLS) and artificial neural networks (ANN). Some examples of sensing techniques and corresponding chemometric models used for quantitative determination of various biological analytes are summarized in Table 1.

Analytes	*Sensing Technique*	*Separation Technique*	*Reference*
Blood components: dopamine, ascorbic acid	Electrochemical (linear sweep voltammetry)	PCR, PLS	[71]
3 antibiotics: ofloxacin, norfloxacin, ciprofloxacin	Electrochemical (linear sweep voltammetry)	PLS, PCR, ANN	[69]
2 hormones: ethinylestradiol, levonorgestrel	Spectrophotometric	PLS, PCR	[72]
Anti-inflammatory drugs: indomethacin, acemethacin, piroxicam tenoxicam	Electrochemical (differential pulse voltammetry)	PLS	[70]
Heart medications: Furosemide, amiloride hydrochloride	Spectrophotometric	PLS	[68]

Table 1. Summary of chemometric models applied to multi-analyte determination

1.3 Thesis Contributions

A chitosan-catechol electrode material coating was tested for its performance in the presence of a common interfering species as well as in the complex serum matrix. In parallel, a systematic methodology incorporating the use of cross-reactive sensors was developed in order to explore and identify interfering species in serum-based sensing. This thesis presents a method for screening, discerning and matching individual interfering species in buffer and serum matrices. The feasibility of this approach was demonstrated using the model analyte, CLZ with the following specific contributions:

a) The selectivity of the chitosan-catechol modified sensor was evaluated.

b) Species present in blood serum were screened using electrochemical methods and tested for statistical significance in order to narrow down potentially interfering species.

c) A set of cross-reactive sensors were characterized to investigate the functionality and ability of each sensor to sense a variety of species and provide diversified responses.

d) The performance of the cross-reactive sensors in providing insight into the effect of interfering species in the CLZ measurement.

e) Application of multi-dimensional mapping of the sensor responses to create patterns that enabled matching of signals from CLZ and interfering species across buffer and complex serum-based matrices.

Chapter 2: Chitosan-Catechol Redox-Cycling System

2.1 Design

2.1.1 Implementation of the Chitosan-Catechol Coating

Chitosan is a polysaccharide that is capable of being controllably electrodeposited onto electrode surfaces by the application of potential energy, to form a hydrogel film. The use of chitosan is advantageous because it can serve as a graft for additional functional elements. For instance, it enables grafting of catechol moieties close to the electrode surface, as shown by Kim et al. [73], which in turn can be used for redox cycling. Redox cycling refers to a type of catalytic behavior, where an electrochemically reversible species can be cycled through a continuous process of oxidation and reduction. By engineering an RCS whereby a species of interest can be continually oxidized by an applied electrode potential and reduced by catechol moieties close to the electrode surface, signal amplification can be achieved via redox cycling. Thus, the ccRCS is amenable as a signal amplification technique for CLZ sensing.

Redox cycling will occur between the electrode and the catechol moieties if the analyte is an oxidizing mediator with a redox potential that is larger than that of catechol (~0.2 V). Thus, CLZ, which has a redox potential of ~0.4 V, is a good candidate for redox cycling amplification by the ccRCS film. Toward the application of the ccRCS for CLZ measurement, the scheme shown in Figure 6 is proposed,

where an electron cascade follows the path of thermodynamic favorability (least resistance). A reducing mediator (hexaammineruthenium; Ru) with an oxidation potential of -0.2 V, can charge the chitosan-catechol film by donating electrons to it. When negative potentials are applied, Ru is reduced so that this source of electrons for the chitosan-catechol film is continuously regenerated during measurement. When positive potentials are applied, CLZ can be oxidized at the electrode. CLZ can then be reduced back to its original state by reacting with the grafted catechol moieties, such that re-oxidation at the electrode occurs. The continuous redox reaction of CLZ between the electrode and the catechol moieties can increase the total charge transferred by CLZ oxidation, amplifying the generated electrochemical current and improving the signal-to-noise ratio.

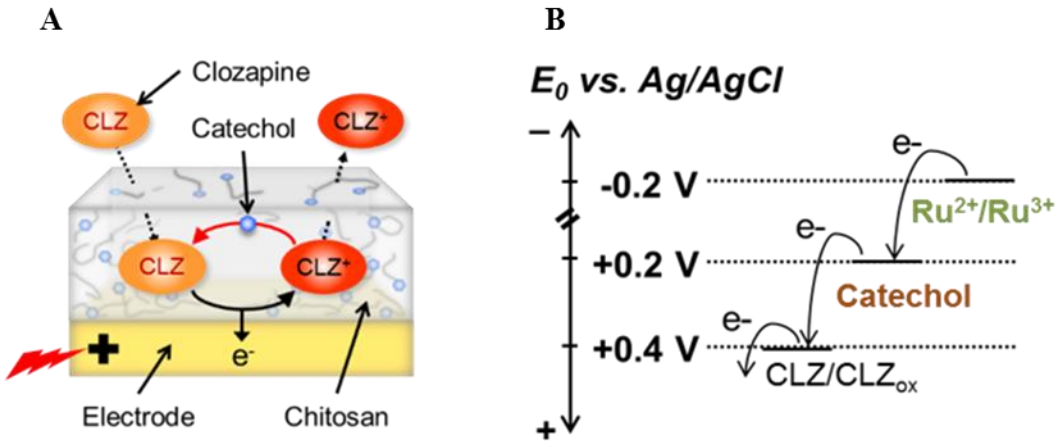

Figure 6. Hypothesized Electrochemical Scheme at ccRCS Electrodes. (A) Scheme illustrating the CLZ electrochemical redox at the RCS. CLZ is thought to undergo redox cycling due to the ability of catechol in the RCS to reduce CLZ and enable repeated CLZ oxidation at the electrode. (B) Electron cascade showing the thermodynamically favored direction of electrode flow.

2.1.2 Previous Work

We have previously demonstrated the use of the ccRCS for CLZ measurement in buffer-based solutions, as shown in Figure 7. In the optimized system, a sensitivity of 54 ± 7 ($\mu C/cm^2$)/($\mu L/mL$) and 7.0 ± 2.6 ($\mu C/cm^2$)/($\mu L/mL$) for catechol-chitosan and bare electrodes, respectively, was achieved. Thus, higher sensitivity values were achieved with the ccRCS, suggesting increased peak current generated by redox cycling of CLZ at the ccRCS (Figure 7b). Preliminary serum-based CLZ measurement show the responses near the therapeutically relevant CLZ concentrations although with higher limits of detection and error compared to buffer-based solutions (Figure 7c). However, signals from the CLZ-spiked serum demonstrate lower performance and require subtraction of the un-spiked serum background signal in order to be resolved. This is not ideal in practice since information about a subject's blood sample without the medication is not typically available. Nonetheless, it demonstrates a first step toward sensing in serum without any pre-treatment steps.

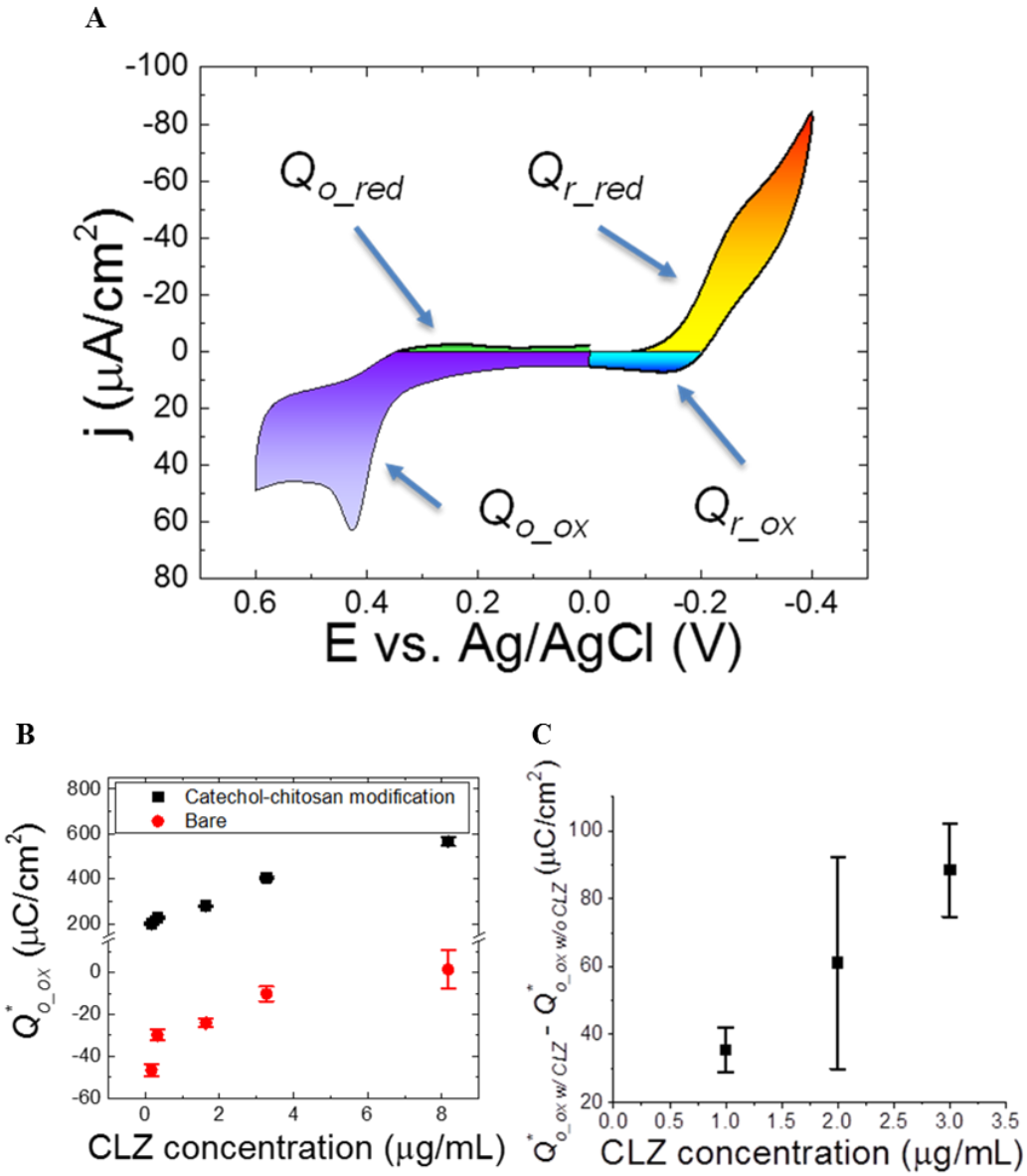

Figure 7. Calibration of CLZ at ccRCS Electrodes. (a) Cyclic voltammogram response divided into 4 sections, Q_{r_red} (red-yellow) for cathodic charge at E < 0 V (Ru reduction), Q_{r_ox} (blue) for anodic charge at E < 0 V, Q_{o_ox} (purple) for anodic charge at E > 0 V (CLZ oxidation), and Q_{o_red} (green) for cathodic charge at E > 0 V. The Q_{o_ox} section was correlated to CLZ concentration in (b) buffer solutions using bare and catechol-chitosan modified electrodes, as well as in (c) serum solutions using catechol-chitosan modified electrodes. Measurements were carried out in duplicates using an on-chip setup [74].

2.1.3 Interference Studies with the Chitosan-Catechol Redox Cycling System

Because CLZ does not have specific biological recognition elements that can be employed to provide selectivity to the assay, interference from other species present in blood serum becomes a critical factor affecting sensor performance. In order to achieve a lower limit of detection of CLZ in serum samples (that covers the entire range of therapeutic CLZ levels) as well as a more sensitive and reliable measurement, the fundamental properties of serum and how they affect the CLZ sensor will be further studied. First, semi-selectivity properties of the ccRCS are studied with a model interfering species (IS), ascorbate (AA) [75], which commonly interferes with electrochemical sensors [13, 14]. Then, a closer examination of the serum responses at the ccRCS was used to assess this material coating with regards to interference.

Even though the ccRCS electrode modification does not provide the selectivity that biological recognition elements possess, it has intrinsic properties that can minimize the effect of interference. Specifically, only species whose oxidation potentials fall between that of catechol (0.2 V) and that of the applied electrode potential can thermodynamically receive electrons from catechol and thus be amplified by oxidative redox cycling. For instance, CLZ, which has an oxidation potential larger than 0.2 V, is shown to undergo redox cycling whereas AA, which has an oxidation potential below 0.2 V, is hypothesized to be unable to receive electrons from the catechol moieties (as illustrated in Figure 8). Furthermore, the ccRCS can only engage molecules that are electrochemically reversible in redox cycling.

Electrochemically irreversible or unstable species (such as AA) would be unable to be reduced and re-oxidized in a redox cycling manner. These properties of the ccRCS enable what we refer to as semi-selectivity of the sensor.

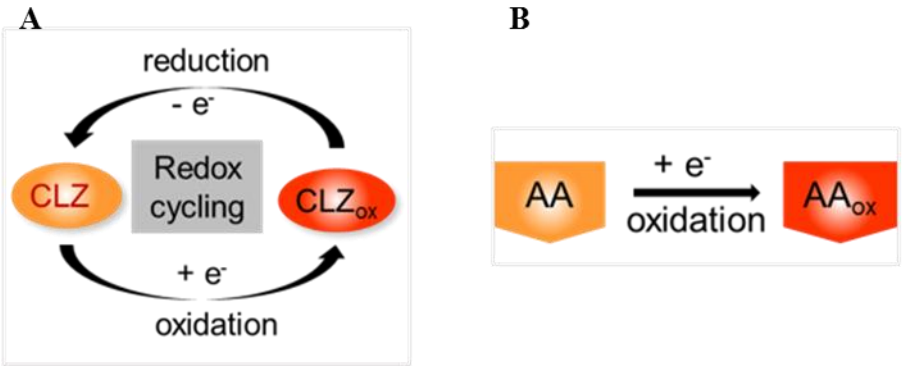

Figure 8. Scheme illustrating the hypothesis for (a) CLZ and (b) AA electrochemical redox at the ccRCS. CLZ is thought to undergo redox cycling due to the ability of catechol in the ccRCS to reduce CLZ and enable repeated CLZ oxidation at the electrode. AA is thought no to undergo redox cycling, likely due to its instability and irreversibility as well as the lack of energetic favorability for redox cycling with catechol in the ccRCS.

2.2 Methods

2.2.1 Electrochemical Cell

Electrochemical tests are carried out in a three electrode cell configuration, unless otherwise stated, using a CHI660D potentiostat (CH Instruments; Austin, TX). The three-electrode cell, illustrated in Figure 9, consists of a 2 mm diameter gold working electrode (CH Instruments; CHI101), a platinum foil counter electrode, and a Ag/AgCl reference electrode (CH Instruments; in 1 M KCl) in a closed cell with 1.6 mL sample solution. The working electrode was polished using 0.05 micron alumina powder before each film fabrication in order to regenerate the surface and remove any adsorbed impurities (*i.e.*, oxides). The surface cleanliness was electrochemically

validated before every test by measuring a model redox couple using a cyclic voltammetry technique (CV: initial and final potential: 0.19 V, potential range: -0.06 V to 0.44 V, scan rate: 0.2 V/s, 6 cycles), and comparing it to previous CV responses. The redox couple solution consisted of 10 mM phosphate saline buffer (PBS), 100 mM sodium chloride, 10 mM ferricyanide and 10 mM ferrocyanide. The typical ferrocyanide/ferricyanide CV response is shown in **Figure 10**a. When responses not consistent with previous ones occur, the electrode surface is polished again until the correct validation response is achieved.

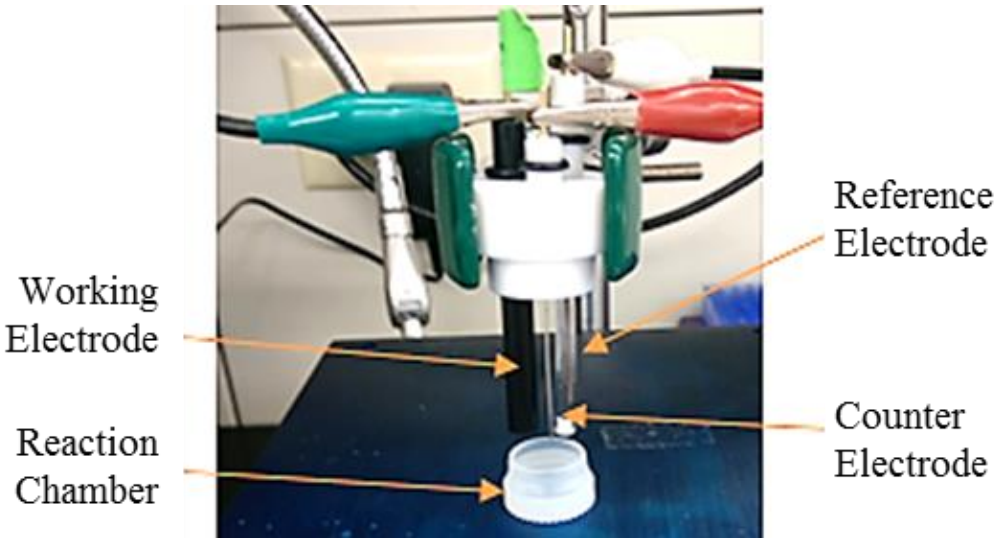

Figure 9. Electrochemical cell composed of a gold working electrode, Ag/AgCl reference electrode, and platinum wire counter electrode. A reaction chamber holding 1.6 mL volume was used.

2.2.2 Chitosan-Catechol Film Fabrication

Film fabrication consists of two consecutive steps: chitosan electrodeposition and catechol grafting. Chitosan (1% solution in dilute HCl; pH 5-6) was electrodeposited on the working electrodes by applying a constant cathodic current of 6 A/m^2 for 45 seconds on the working electrode, followed by rinsing with phosphate buffer saline

(10 mM PBS; pH 7) solution to form a clear hydrogel around the electrode. Next, catechol (5 mM solution in 0.1M phosphate buffer (PB; pH 7.0)) was grafted onto the chitosan film by applying a constant positive potential of 0.6 V for 3 minutes, followed by immersion in water for 5 minutes to discard unbound catechol. This process forms chemical bonds between the chitosan film and the catechol moieties. The electrochemical responses of the chitosan electrodeposition and catechol grafting are shown in **Figure 10**b and c, respectively. A new film was generated for each sensing measurement.

2.2.3 Electrochemical Validation

Following film fabrication, another validation step was employed to ensure minimal between-electrode variability. The validation tests employed a CV (initial and final potential: 0 V, potential range: -0.4 V to 0.7 V, scan rate: 0.1 V/s, 7 cycles) using a solution of 25 μM 1,1'- ferrocenedimethanol (Fc) and 25 μM hexaammineruthenium (III) (Ru) in 0.1 M PB (pH 7.0) solution. Fc serves as an oxidizing mediator which discharges the ccRCS film, and Ru serves as a reducing mediator which charges the film. When the redox response matches the Fc/Ru response from previous ccRCS modified electrodes (**Figure 10**d), it can be assumed that the film properties are similar to those of previous films, thereby validating the fabrication process.

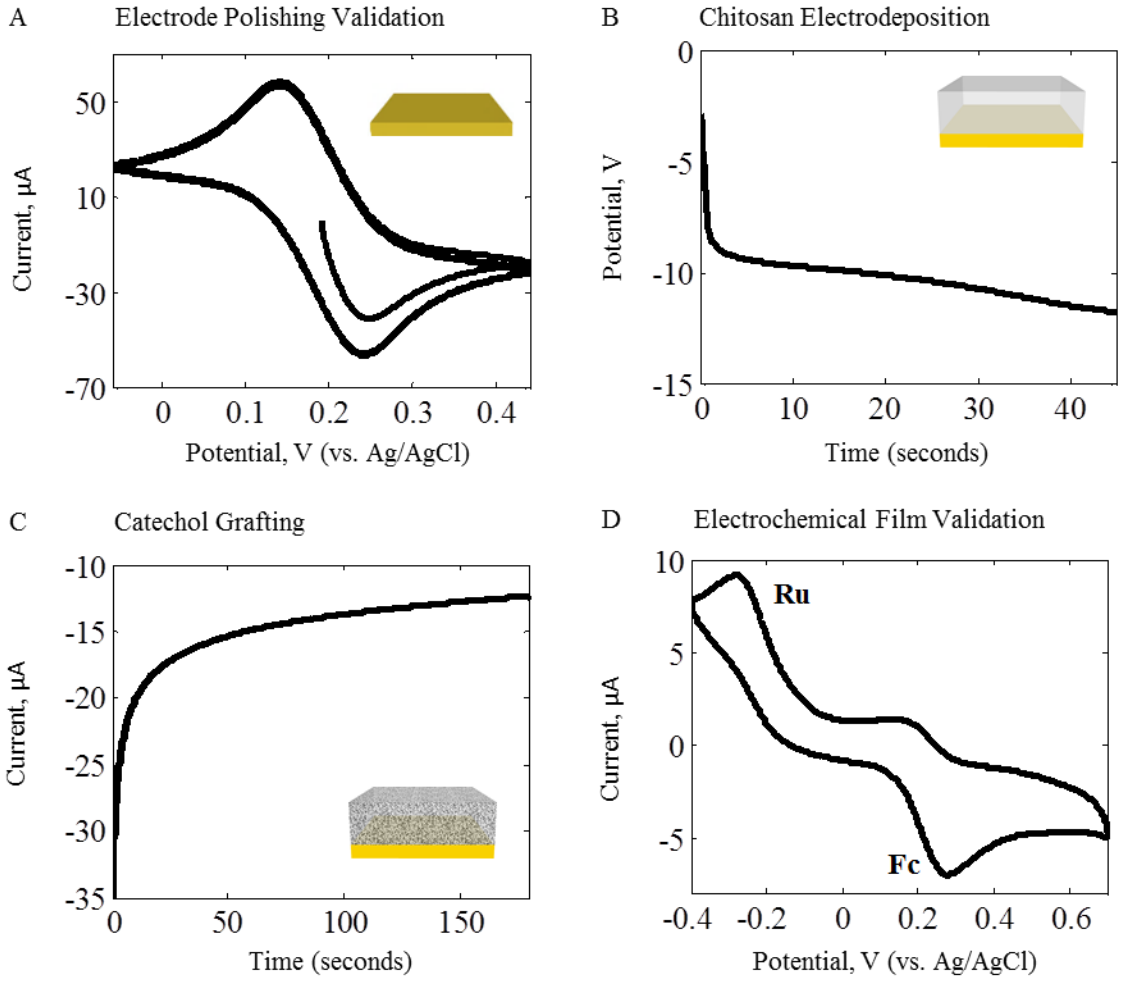

Figure 10. Electrochemical responses of the fabrication and validation steps for chitosan-catechol electrode modification: (a) cyclic voltammogram for Ferrocyanide/Ferricyanide redox species used for validating regeneration of the electrode surface after polishing, (b) chronopotentiometry for chitosan electrodeposition, (c) chronoamperometry for catechol grafting, and (d) cyclic voltammogram for Fc/Ru chitosan-catechol film validation (last cycle shown). The gold-colored surface in the inset illustrations represents the commercial gold electrode, the transparent gray-colored rectangle represents the chitosan hydrogel and the black dots embedded in the hydrogel represent the catechol moieties.

2.2.4 Electrochemical Clozapine Measurement in Buffer

Electrochemical testing was performed with solutions of 25 µM CLZ, 25 µM Ru, and 100 µM ascorbic acid (AA) in 0.1 M PB (pH 7) using a cyclic voltammetry (CV) technique (initial and final potential= 0 V, potential range: -0.4 V to 0.7 V, negative initial scan polarity, scan rate = 0.01 V/s, 7 sweep segments, sample interval 0.001

V). All samples were purged (bubbled) with nitrogen gas for 10 minutes before electrochemical measurements to remove dissolved oxygen. This step is important in the characterization stage because it ensures less background noise in the CVs response. Data was processed by subtracting the 0.1 M PB background signal obtained with bare gold electrodes from each sample response and the last CV cycle is shown.

2.2.5 Electrochemical Clozapine Measurement in Serum

Commercial human blood serum (from human male AB plasma, USA origin, sterile-filtered, Sigma Aldrich) was divided into 1 mL aliquots and stored in -20 °C conditions. Prior to the experiment, the serum was thawed at room temperature. Commercial undiluted serum was spiked with 25 µM Ru and 10 µM CLZ concentrations immediately before testing.

The CLZ-spiked serum samples were tested using a lab-on-a-chip platform [74]. Briefly, an on-chip electrochemical cell containing a gold working electrode (WE; disk-shaped, 1.5 mm radius), a gold counter electrode (CE), and a reference Ag/AgCl reference electrode (RE) was defined by a patterned photoresist, resulting in a chamber with 4.5 mm radius and height of 22 µm. The on-chip open Ag/AgCl RE is fabricated by a 2-step electrodeposition method: 1) Ag electroplating on the patterned Au electrode, 2) AgCl generation on the Ag electrode surface [76]. The electrochemical measurement consisted of a CV technique (initial and final potential:

0 V, potential range: -0.4 V to 0.6 V, scan rate: 0.02 V/s, 1.5 cycles). All electrochemical tests were done in duplicates and the average is shown.

2.3 Experimental Results

2.3.1 Clozapine Detection with Bare Gold Electrodes

As seen in Figure 11, the CV response of CLZ with gold electrodes (before surface modification) shows a primary reversible redox reaction near 0.38 V, and a secondary reversible redox reaction near 0.18 V corresponding to the electroactive CLZ byproduct, as described in section 1.2.3.3. The four peak responses of CLZ illustrate a pattern with respect to peak location that is characteristic to this species.

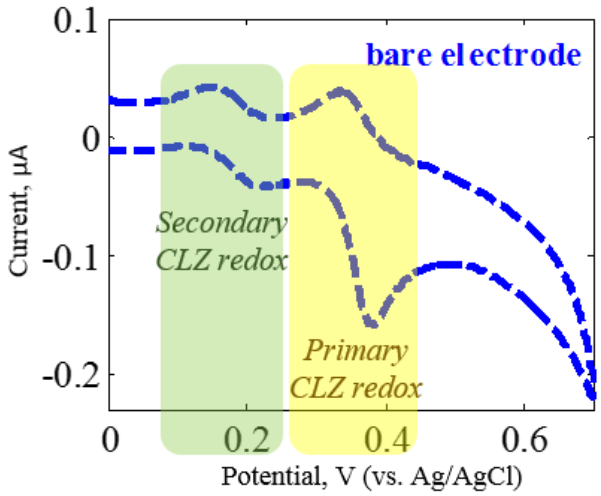

Figure 11. Cyclic voltammograms of 25 µM CLZ oxidizing mediator in the presence of 25 µM Ru reducing mediator in PB solutions (pH 7.4) using bare (no surface modifications) gold electrodes. Negative currents represent oxidation and positive currents represent reduction.

2.3.2 Clozapine Detection with Chitosan-Catechol Redox Cycling System

The ability of the ccRCS to amplify the oxidation response of CLZ is shown in Figure 12, in a cyclic voltammogram with a solution containing CLZ and Ru. From the figure, a marked increase in electrochemical current for the CLZ oxidation becomes immediately apparent, illustrating the amplification benefits of the ccRCS. The gain in signal can be quantified with an amplification factor of 9.2, derived using equation 5 given below.

(5) $$amplification\ \ factor = AF = \frac{\left(I_{peak\ with\ CLZ} - I_{peak\ without\ CLZ}\right)_{Chitosan-catechol}}{\left(I_{peak\ with\ CLZ} - I_{peak\ without\ CLZ}\right)_{BareAu}}$$

The CLZ amplification observed with modified electrodes is due to the donation of electrons from catechol moieties to CLZ molecules. This electron transfer reduces the CLZ back to its original form, enabling each CLZ molecule to be oxidized multiple times at the electrode surface. The sustained cycling of CLZ oxidation (at the electrode) and reduction (at the catechol) constitutes the redox cycling of CLZ, which amplifies the CLZ oxidation signal. Moreover, the oxidation potential of CLZ is observed to shift from 0.38 V in bare electrodes 0.48 V in modified electrodes, as seen in Figure 12, likely due an increased uncompensated resistance from the physical boundary created by the chitosan film, which decreases the diffusion of CLZ to the electrode surface. Similarly, the Ru signal is also amplified in the ccRCS modified electrode since catechol oxidizes Ru as it is charged, generating more reducible Ru species in the presence of catechol.

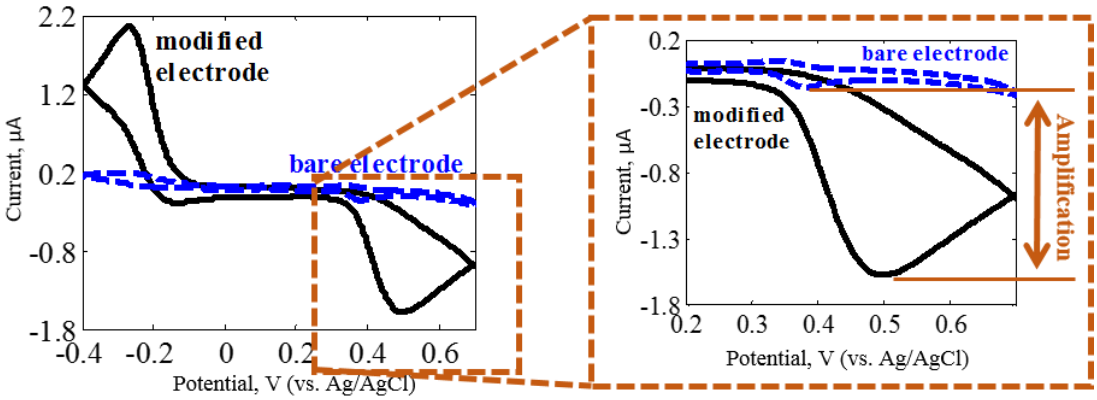

Figure 12. Cyclic voltammograms of 25 µM CLZ oxidizing mediator in the presence of 25 µM Ru reducing mediator in PB solutions (pH 7.4) using bare (no modification) and ccRCS modified gold electrodes, showing an amplification factor of 9.2 of CLZ with the modified system.

2.3.3 Interference Study with Ascorbate

The electrochemical behavior of AA (100 µM) and CLZ (25 µM), individually and mixed, were studied. They are first analyzed on bare electrodes to understand the intrinsic behavior of each species in a simple system. As shown in Figure 13, AA has an oxidation peak at 0.18 V, whose tail overlaps with the sharper CLZ peak at 0.38 V due to the broad width and the larger relative peak current of AA compared to CLZ. When AA and CLZ are measured simultaneously, the CLZ peak current increases 1.8-fold compared to the response of CLZ individually. It is ambiguous whether ascorbic acid is amplifying the CLZ peak by donating electrons to it or interfering with the system due to a peak overlap. In either scenario, the CLZ signal appears to be dependent on the ascorbic acid response, which may be a challenge because the AA concentration in serum can vary across the population.

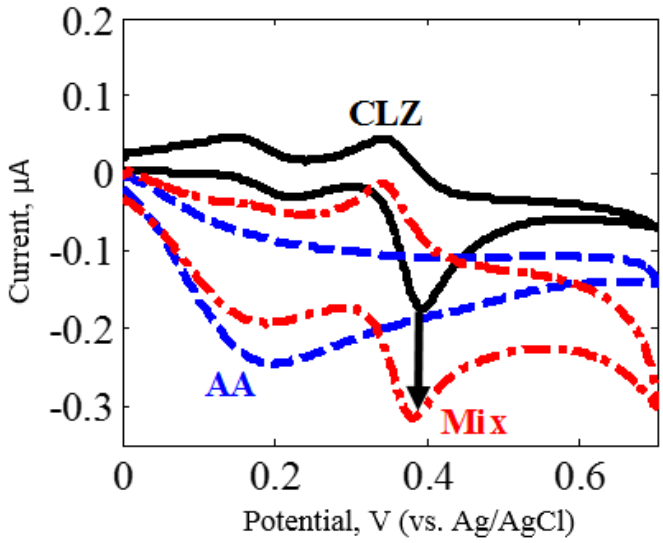

Figure 13. Cyclic voltammograms of 25 µM CLZ and 100 µM AA individually and in mixture (mix), in PB solutions (pH 7.4) using bare gold electrodes. The figure shows the interference from the AA on the CLZ oxidation peak as a change in peak amplitude.

The ccRCS-modified electrodes show a significant increase in the CLZ peak response (AF = 9.2) for ccRCS compared to unmodified electrodes but less amplification for AA (AF = 1.6) in Figure 14a. In fact, whereas the response of AA was larger in the unmodified electrodes compared to the CLZ response, the opposite occurs for the ccRCS. Thus, the ccRCS indeed has the capability of semi-selective amplification of CLZ compared to AA. Furthermore, when CLZ and AA are simultaneously present, the oxidation peak current of CLZ is not significantly affected by the presence of AA. In the presence of AA, the CLZ peak increases only by 1.15-fold compared to the individual CLZ peak, compared to a 1.8-fold increase in the bare electrode. Lastly, when measuring the overall effect of AA in the complete ccRCS for CLZ measurement, where Ru film charging agent is present, no apparent difference is seen in the presence or absence of AA, as shown in Figure 14b. Thus, the ccRCS can minimize selectivity issues encountered in unmodified gold electrodes with its semi-selective signal transduction.

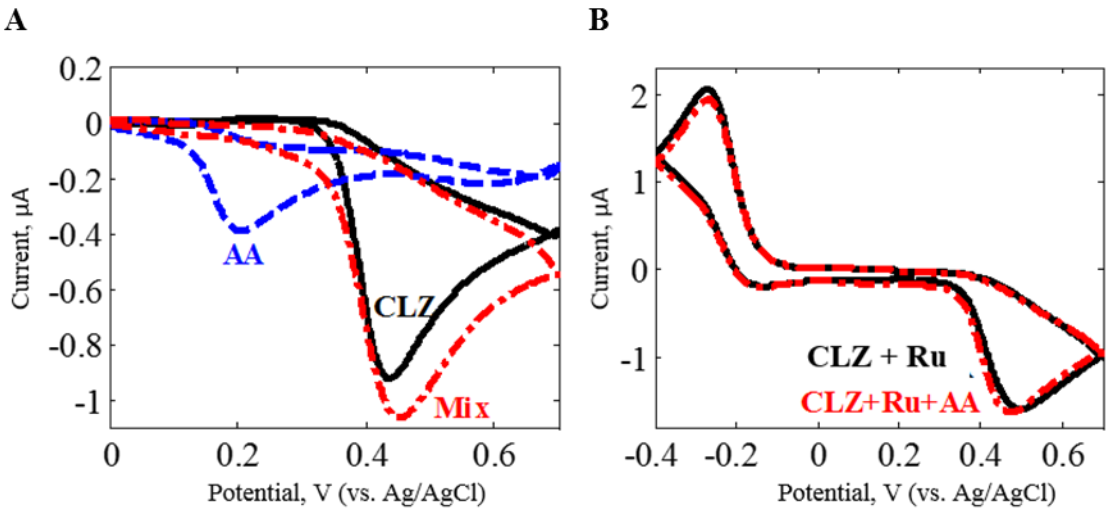

Figure 14. Cyclic voltammograms of (a) 25 µM CLZ and 100 µM AA individually and in mixture, in PB solutions (pH 7.4) using ccRCS modified gold electrodes, showing increased amplification of the ccRCS for CLZ compared to AA. (b) Effect of AA on the overall CLZ measurement using the ccRCS, when the 25 µM Ru film charging agent is present.

2.3.4 Interference Studies with Serum

As seen in Figure 15, the CV of the background untreated serum current response exhibits two peaks at 0.42 V and 0.51 V. This result is extremely important because these background signals occur in the vicinity of the CLZ oxidation signal. Moreover, the addition of CLZ to blood serum led to a peak overlap with the background signal. An incremental increase in response compared to the background peak is observed in the presence of CLZ, where the background peak is dominant likely due to lower concentration of CLZ compared to the concentration of background species.

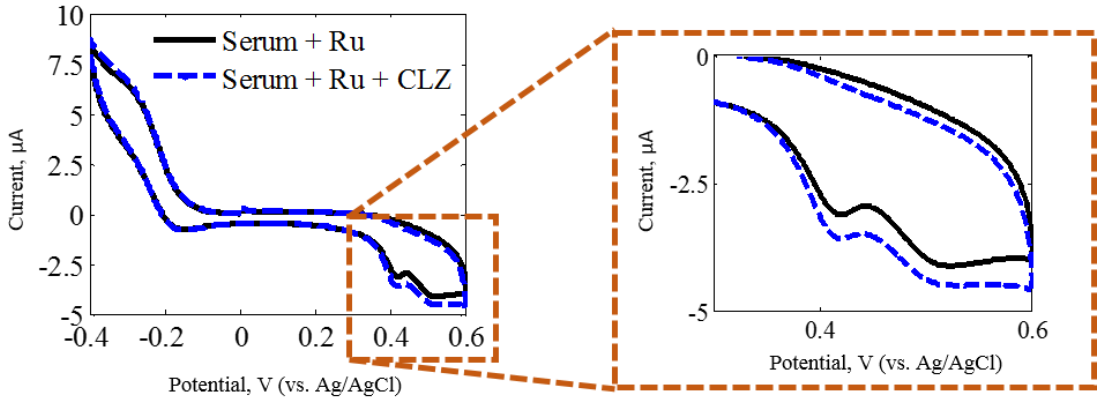

Figure 15. Cyclic voltammograms of untreated blood serum spiked with Ru reducing mediator, with and without 10 µM CLZ at the ccRCS modified elecrode. The figure shows the background peaks that overlap the CLZ oxidation peak and become convoluted. The lab-on-a-chip device was used for these measurements.

In contrast to AA, interferences from other species in blood serum were not rectified by this sensor design configuration. Some suggestions for improving the sensor performance in blood serum include identifying the interfering species from the sample matrix, incorporating a sensor material that creates a barrier for the interfering species to the sensor surface, or employing a different type of sensor whose mechanism targets the differentiation of the particular interfering species in the sample. Nonetheless, these suggestions require knowledge of the species involved in the background serum signal and/or CLZ interference.

2.4 Summary

The ccRCS modified electrodes were shown to amplify CLZ electrochemically 9.2-fold compared to unmodified electrodes. This amplification capability improves the signal-to-noise ratio, which can enable increased sensitivity for low-concentration CLZ measurements. Furthermore, the selectivity studies of the ccRCS studied for

CLZ and AA common interfering species indicated that the ccRCS did not amplify the AA signal, demonstrating semi-selectivity for CLZ. However, other interfering species in blood serum were seen to interfere with the CLZ measurement and require further studies.

To improve the selectivity and performance of a CLZ sensor for serum measurement, a broader interference study would be useful to identify and account for interference from the numerous species simultaneously present in blood serum, especially in the case of semi-selective (rather than fully selective) sensors, where interfering species can have significant effects on the analyte measurements. This methodology can enable a more targeted sensor design for CLZ to account for the relevant interfering species, and its development is described in the next section. The results can provide guidelines for improving the selectivity of the ccRCS (and a broader set of sensors) in the measurement of CLZ in serum.

Chapter 3: Screening of Interfering Species in Blood Serum

3.1 Design

Some of the endogenous and exogenous species present in blood serum are redox-active and can interfere with the CLZ measurement via cross-reactions or signal overlap, for instance. Due to the lack of highly selective biorecognition elements for CLZ and the complexity of human blood serum, a method of identifying serum species that interfere with the CLZ measurement was developed.

The design for a systematic methodology for interference screening and characterization is presented. It consists of screening species present in serum individually by testing their electrochemical response in buffer solutions. This step consists of testing a carefully selected set of endogenous species with respect to their effect on the CLZ measurement. Assessment of the electroactivity of these species tested individually and in simulated mixtures (CLZ + individual species) can be used to characterize the effects from the simultaneous presence of multiple species in solution. In the next chapter, a comparison between buffer-based individual species to serum responses is used to match response signals of serum to individual species. By combining buffer-based screening with serum-based testing, we can expect to identify and validate endogenous serum species with significant interference to the CLZ measurement in serum-based solutions. Once identified, their inter-dependence can be determined such that the interference can be accounted for in the design of sensor system.

3.2 Methods

3.2.1 Interference Screening

A list of potential interfering species (IS) were screened at their upper physiological concentrations as suggested in the CLSI EP7-A2 guidelines [77], and those that interfere with the CLZ measurement were further characterized. Initially, we will consider the following classes of species as potential IS: 1) most abundant metabolites [78, 79], and 2) low-molecular weight species that interfere in similar sensors, as shown in Table 2. The latter includes electrochemical sensors for other CLZ sensing schemes as well as other analytes sensed in the measured potential range of 0 – 0.7 V [13, 37, 80-86].

Criteria	***Interfering Species***	***Upper Concentration, μM***
Analyte	Clozapine	5.6
Most Abundant Organic Metabolites	D-Glucose	6100
	Urea	9000
	ATP	3000
	DL-Glyceraldehyde	1500
	L-Lactic Acid	2400
	L-Glutamine	670
	L-Alanine	410
	Glycine	282
	L-Lysine	217
	Uric Acid	410
Interference Found in Similar Measurement Techniques	Ascorbate	40
	L-Cysteine	60
	L-Valine	276
	L-Arginine	140
	L-Glutamic Acid	150
	L-Methionine	40
	Oxalic Acid	22

Table 2. Chosen species and upper physiological concentrations used to screen species that interfere in blood serum samples.

.

To test the extent of interference of various endogenous species with CLZ, the electrochemical response of simulated mixtures (individual IS + CLZ) in PBS buffer based solutions were compared to that of CLZ-only solutions, and expressed as a differences in their electrochemical peaks. A one-way ANOVA test between the two sample populations was carried out for two characteristic peak values, peak current and peak potential. The significance threshold was chosen to be $\alpha = 0.1$ for the peak current and $\alpha=0.01$ for the peak potential since the latter has intrinsically less variation. Using this screening approach, species posing significant effects to the CLZ peak were identified.

3.2.2 Electrochemical Test Setup

A glassy carbon disk working electrode (GCE, 3 mm diameter), a platinum wire counter electrode, and a Ag/AgCl (1 M KCl) reference electrode were purchased from CH Instruments. Electrochemical tests were performed with a CHI660D potentiostat (CH Instruments) All potential values presented are written in reference to a Ag/AgCl half-cell potential. The working electrodes were cleaned by successively polishing with 1, 0.3, and 0.05 µm alumina powders and were electrochemically validated before every test. Validation was performed as in section 2.2.3. A differential pulse voltammetry technique (DPV: initial E = 0 V, final E = 0.7 V, increment E = 0.001V, amplitude = 0.05 V, pulse width = 0.2 s, sampling width = 0.0167 s, pulse period = 0.5 s) was employed. All species were dissolved tested in PBS (pH 7.4) solutions.

3.3 Experimental Results

Individual species were systematically screened for electroactivity at their upper physiological concentration. Only four components were shown to be electrochemically active (Table 3): uric acid (UA), L-cysteine (CySH), ascorbate (AA) and oxalic acid (OA). One common theme among the former three species is their antioxidant properties [87-89], with UA accounting for a majority of antioxidant capacity [90]. This result suggests that antioxidants are amenable to electrochemical detection and may be a source of interference in blood serum. Additionally, UA, CySH and OA have electrochemical peak potentials similar to that of CLZ as seen in Figure 16, thus their peak response is most likely to overlap or affect the CLZ measurement.

Interfering Species	$\bar{E}_{p,IS}$ **(V)**
Clozapine	0.34
Uric Acid	0.245
Ascorbate	< 0.08
L-Cysteine	0.347
Oxalic Acid	~0.36

Table 3. Interference Screening: Part 1-Electroactivity. Electrochemical oxidation peak values ($\bar{E}_{p,IS}$) of potentially interfering species with detectable electroactivity. Triplicate tests were carried out using a bare glassy carbon working electrode in buffer-based solutions (pH 7.4), and the average values are shown.

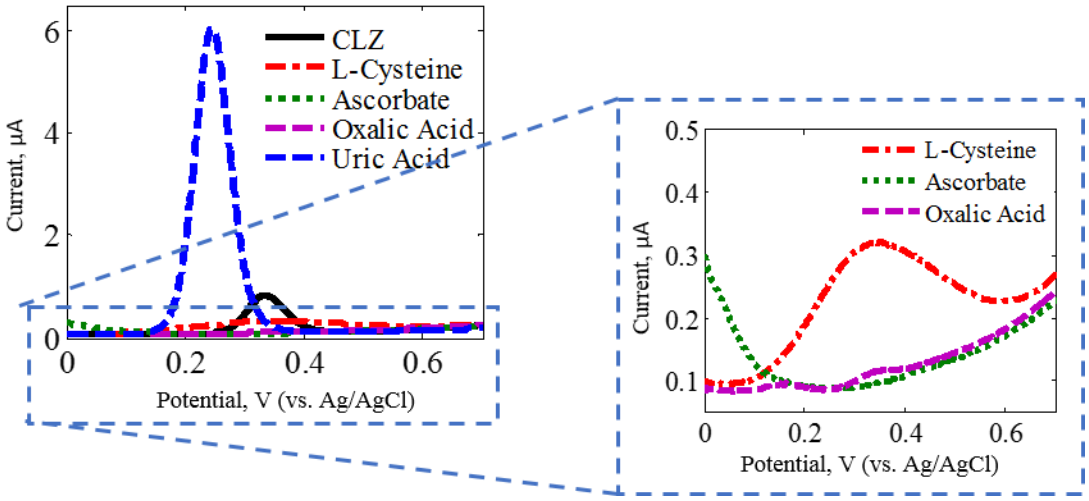

Figure 16. Differential pulse voltammetry (DPV) of 60 µM L-cysteine, 410 µM uric acid, 22 µM oxalic acid, and 40 µM ascorbate (pH 7.4) in PBS at the GCE. Signal response represents an average of triplicate measurements.

Cross-reactivity between these endogenous species and the CLZ exogenous species was screened. The electrochemical signals from simulated mixtures (individual endogenous species + CLZ) and CLZ-only solutions in buffer were compared to assess the effect of the simultaneous presence of the two components on the CLZ response. The cross-reactivity is represented in terms of the signal difference of the mixture and the CLZ-only solution (bias) as well as the corresponding *p*-values obtained from a one-way ANOVA test between the two samples (as described in section 3.3.1). As seen in Table 4, UA and CySH were found to have significant cross-reactivity with CLZ with respect to both peak current and peak potential (p-values < threshold).

		Mixture = Interfering Species + Clozapine			
	Interfering Species	**$I_{p,mix}$ Bias (µA)**	***p*-value of $I_{p,mix}$ Bias**	**$E_{p,mix}$ Bias (V)**	***p*-value of $E_{p,mix}$ Bias**
Analyte	Clozapine	--	--	--	--
Most Abundant Organic Metabolites	D-Glucose	-0.07423	0.1858	-0.0037	0.2505
	Urea	-0.0699	0.3135	-0.0047	0.0325
	ATP	-0.0206	0.7888	-0.0030	0.4557
	DL-Glyceraldehyde	-0.0571	0.5287	-0.0003	0.9465
	L-Lactic Acid	-0.0832	0.1443	-0.0030	0.4103
	L-Glutamine	-0.0362	0.4611	-0.0037	0.2913
	L-Alanine	-0.0574	0.3265	-0.0037	0.0254
	Glycine	-0.0680	0.2230	-0.0040	0.0705
	L-Lysine	0.0661	0.1224	-0.0020	0.1447
	Uric Acid	**5.0160**	**$9.02*10^{-7}$**	**-0.0843**	**$1.69*10^{-6}$**
Interference Found for Similar Measurement Techniques	Ascorbate	-0.0111	0.8571	0.0007	0.8309
	L-Cysteine	**-0.3175**	**0.0068**	**-0.0487**	**$2.09*10^{-5}$**
	L-Valine	0.0120	0.8406	0.0023	0.2564
	L-Arginine	-0.1052	0.1357	-0.0053	0.3671
	L-Glutamic Acid	-0.0139	0.7502	0.0013	0.4918
	L-Methionine	0.0030	0.9520	0.0013	0.6918
	Oxalic Acid	-0.0492	0.5661	0.0020	0.4885

$I_{p,mix}$ Bias = $\Delta I_{p,mix} = |\overline{I_{p,Mixture}}| - |\overline{I_{p,CLZ}}|$, where $\overline{I_{p,i}}$ represent the mean peak current of CLZ or Mixture (CLZ + interfering species) of the triplicate results.
$E_{p,mix}$ Bias = $\Delta E_{p,mix} = \overline{E_{p,Mixture}} - \overline{E_{p,CLZ}}$, where $\overline{E_{p,i}}$ represent the mean peak potential of CLZ or Mixture (CLZ + interfering species) of the triplicate results.
* Note: the corresponding CLZ peak in the mixture was determined as the detectable peak closest to the individual CLZ peak. The *p*-value refers to the results of an ANOVA test between clozapine alone and in mixture.

Table 4. Interference Screening: Part 2. Statistical analysis of interference imparted on the clozapine measurement by interfering species. Triplicate tests were carried out using a bare glassy carbon working electrode in buffer-based solutions (pH 7.4). The average values are shown.

3.4 Summary

A systematic selection and coarse screening methodology was applied for identifying species that are present in blood serum which affect the electrochemical CLZ measurement. The method consisted of first selecting species with highest abundance and species known to interfere in similar sensors at the range of applied potentials,

which enabled narrowing down from hundreds of species present in blood serum to 17. Then, electrochemical tests were carried out with and without the presence of each individual species, and only 2 species were identified for interference with the CLZ measurements: UA and CySH. Having narrowed down the interfering species, studies in Chapter 4 are focused on the interaction of UA and CySH with CLZ and how their integrated response in serum affects the CLZ measurement.

Chapter 4: Using Cross-Reactive Sensors to Characterize Interfering Species

4.1 Design of Cross-Reactive Sensors

4.1.1 Overview

Sensor arrays have been used as part of a concept known as the artificial tongue and nose to enable multi-analyte assessment in complex mixtures by coupling it with signal processing (*i.e.*, chemometric) models, as discussed in section 1.2.4. Furthermore, many articles have demonstrated the ability of such systems to resolve overlapping peaks and account for multiple analytes (*i.e.*, significant interferences) in complex fluids. This method relies on a series of CRSs that each provides diverse and synergistic information regarding the analyte(s) of interest. Thus, the diversity of a sensor array provides a multi-dimensional perspective that accounts for variable background and interfering signal responses in blood. However, knowledge of the major causes of background variability and interference in the sample allows for more efficiently calibrating the sensor system and chemometric models.

A set of cross reactive sensors that have the capability of providing orthogonal multi-dimensional responses to create an electronic tongue type sensor is proposed. The CRSs were designed to be amenable to miniaturization and provide differential signal responses. It consists of variations in the sensing method, such as electrical input, pH and material, as specified in Table 5. Each sensing method was designed to provide different or additional signatures of an individual or a combination of measured

species. Signatures across the array could be represented in the form of integrated multi-dimensional plots that map the overall signature of the sensor array and facilitate comparison between samples. Further description of the choice of each sensing method is given in the following sections.

Sensing Method	Electrode Material	Electrochemical Technique	pH
A	GCE	DPV	7.4
B	GCE	DPV	**6.5**
C	GCE	DPV	**8.0**
D	GCE	**CV, oxidation, cycle 1**	7.4
ΔD	GCE	**CV, oxidation, difference between cycles**	7.4
E	GCE	**CV, reduction, cycle 1**	7.4
F	**Pt**	DPV	7.4

Table 5. Experimental conditions for the CRS set, with elements A-F used to generate various sensor responses. GCE refers to glassy carbon electrodes, Pt to platinum electrodes, DPV refers to differential pulse voltammetry and CV refers to cyclic voltammetry.

4.1.2 Electrochemical Techniques

Differential pulse voltammetry (DPV) is an electrochemical technique with superior resolution of its peak signal. DPV consists of applying a linear potential ramp (dE/dt) superimposed with a series of constant pulses. ΔE is the difference of the pulse and the baseline. Current is taken twice per pulse, before the start and at the end of the pulse, and the difference is measured. This pulsed electrochemical method minimizes the effect of non-faradaic (i.e., electrode surface charging) current on the signal output, such that a clean background signal independent of the electrochemical sweep history is achieved. The peak current response I_p (A) from the DPV technique is directly proportional to the analyte concentration $C_{analyte}$ (mol/cm^3) and pulse amplitude ΔE_p (V), following the Osteryoung-Parry equation:

(2) $$I_p = \frac{n^2 F^2 A}{4RT}\left(\frac{D}{\pi t}\right)^{1/2} C_{analyte} \Delta E_p$$

where n is the number of electrons exchanged, F is the Faraday constant (96487 C/mol), A is the electrode surface area (cm^2), R is the gas constant (8.314 J/K*mol), T is the temperature (K), D is the solute diffusion coefficient (cm^2/s), and t is the time between pulses (s) [91].

The cyclic voltammetry (CV) electrochemical method can provide additional information to the DPV technique. CV is the most common technique for studying dynamic electrochemistry, and is useful for discerning kinetics, rates and reaction mechanisms [91]. CV consists of a (non-pulsing) linear potential sweep performed in cycles spanning the anodic and cathodic potential directions at a scan rate of v. Thus, the CV shows oxidation as well as reduction responses, the added information regarding reduction reactions. If peaks of similar shape are seen in both cathodic and anodic directions of the CV, a species is considered reversible. Various levels of reversibility can occur, such as fully reversible (*i.e.*, ferrocyanide/ferrocyanide redox couple) and semi-reversible reactions (*i.e.*, CLZ), where some of the oxidized species cannot be reduced back again. Additionally, multiple CV cycles allow dynamic visualization of byproducts formed over time, which provide an additional signature that can be related to degradation and side-reactions of the analyte. Dynamic information such as the rate of change of the current response over cycling (element ΔD) are taken into account as well as the magnitude of the peak current I_p (A), which depends on bulk analyte concentration $C_{analyte}$ (mol/cm^3) and scan rate v (V/s), according to the Randles-Sevcik equation as follows:

(3) $$I_p = 0.4463nFA(\frac{nFDv}{RT})^{1/2}C_{analyte}$$

where n is the number of electrons exchanged, F is the Faraday constant (96487 C/mol), A is the electrode surface area (cm^2), R is the gas constant (8.314 J/K*mol), T is the temperature (K), and D is the solute diffusion coefficient (cm^2/s) [91].

4.1.3 pH Adjustment

Because the solution pH can affect the oxidation peak potential of the species in solution, pH was chosen as a parameter that may be able to generate differential electrochemical signals. The E_p (V) dependence is a function of the pH and the specific potential of the species at standard conditions E^o (V) according to the Nernst equation:

(4) $$E_p = E^o - \frac{2.3RTm}{nF}pH$$

with gas constant R (J K^{-1} mol^{-1}), temperature T (K), the ratio of protons m to electrons n transferred during the redox reaction, and Faraday constant F (C mol^{-1}). The Nernst equation (equation 4) assumes a reversible redox reaction, fast kinetics, involvement of protons in the redox reaction and the concentrations at the electrode surface to be in equilibrium with the potential. These assumptions are not completely met for the semi-reversible, slow reaction of CLZ but equation 4 serves as a general guideline. Changes of the pH can also affect pH-dependent functional groups within the GCE surface that can lead to differences in attraction/repulsion forces, reaction kinetics or the reaction mechanism. An additional factor is the effect of pH on the

species solubility. Thus, by using sensing methods to account for various sample pH values, fitted trends can aid in defining characteristic species-specific signatures. For instance, because the CLZ reaction is proton-dependent, we expect its response across varying pH to follow the Nernst equation (equation 4) such that the peak potential of the response changes with pH. By fitting the CLZ responses at varying pH's to the Nernst equation we can obtain an intercept value characteristic of the CLZ standard potential and a slope value corresponding to the ratio of protons to electrons involved in the CLZ oxidation process. It is expected that these values will differ from one species to the others based on their characteristic properties, such as reaction rates and processes.

4.1.4 Electrode Material

Previous work with artificial tongues have successfully employed CRS arrays combining various metals and carbon electrodes [56]. The properties of an electrode material can affect molecular interactions (*i.e.*, attraction/repulsion) between the electrode and species being measured, which can in turn affect the selectivity of the sensor [92].

Attraction/repulsion forces between surface structures of glassy carbon electrodes (GCE) and species in solution can affect reaction kinetics [93, 94]. Moreover, studies have shown that species containing amine groups can form carbon-nitrogen linkages with the GCE surface after oxidation of the amine group to the corresponding cation radical [95, 96]. The level of substitution of the amine plays a major role in the

electrochemical oxidation kinetics as well as in the GCE linkage. For instance, tertiary amines have been found to have most facile oxidation but an undetectable degree of binding to the GCE, likely because of steric hindrance [96]. Furthermore, secondary and primary amines have the least facile oxidation but can better form carbon-nitrogen linkages with GCE [96]. Additionally, metallic electrode materials, such as Pt, undergo different surface reaction processes (adsorption, kinetics, surface oxidation) compared to the carbon-based GCE [97, 98]. Platinum (Pt), has been previously shown to provide orthogonal information in an array of several electrode materials [99].

4.2 Methods

4.2.1 Electrochemical Methods: DPV and CV

A differential pulse voltammetry technique (DPV), as described in section 3.2.2, was employed for elements A – C and F of the CRS set. A cyclic voltammetry technique (CV: initial E and final E= 0 V, high E = 0.7 V, low E = 0 V, positive initial scan polarity, scan rate = 0.01 V/s, 6 sweep segments, sample interval 0.001 V) was used for elements D – E of the CRS set.

4.2.2 Electrode Material

A glassy carbon disk electrode (GCE, 3 mm diameter), a platinum disk electrode (Pt, 2 mm diameter), a platinum wire electrode, and a Ag/AgCl (1 M KCl) electrode were purchased from CH Instruments. Electrochemical tests were performed with a

CHI660D potentiostat (CH Instruments) in a three-electrode configuration of either GCE or Pt as the working electrode, platinum wire as the counter electrode and Ag/AgCl as the reference electrode. All potential values presented are written in reference to a Ag/AgCl half-cell potential. The working electrodes were cleaned by successively polishing with 1, 0.3, and 0.05 µm alumina powders and were electrochemically validated before every test. Validation was performed as in section 2.2.3.

4.2.3 pH Changes

For elements A – C of the CRS set, the pH of PBS and serum were changed according to the sensing element designated value by adding 1 M HCl or 1 M NaOH under mixing conditions, and ensuring a pH within +/- 0.2 units. The pH was measured using a digital Extech Oyster pH meter, calibrated daily.

4.2.4 Multi-Dimensional Mapping using Heat Maps

MATLAB (R2013b) was used to create heat map representations of the electrochemical responses, using the "imagesc" tool. Heat maps show the electrode potential on the x-axis and the CRS sensing elements on the y-axis, with the electrochemical current response amplitude shown as a color scale. This visualization method facilitates comparison of various samples or electrodes. All signals represented by heat maps were processed by taking the absolute value and mean-centering, such that larger positive signals correlate to larger responses (whether it is a reduction or oxidation response). The measured electrochemical signal was

averaged for 20 mV intervals to assemble the response into 35 groups, and this smoothed data is shown in the heat maps. For elements D – F, the electrochemical signal in the presence of analytes was subtracted by the signal of the PBS buffer solution in the absence of the analytes, to improve the heat map resolution. Element ΔD represent the difference between the first and third cycle responses of the cyclic voltammogram, with positive values representing an increase of the electrochemical current response between cycles, and negative values representing a decrease of the electrochemical response between cycles.

A second level of simplification was employed to the heat maps such that only the pattern of peak locations and widths is shown. This visualization of the CRS set enables overlapping various signal patterns for comparison. The peak locations and widths were determined using the second derivative of fitted response curves. To determine the onset and end of a peak, the locations where the curvatures of the peak response change (where the second derivative changes signs) were determined in MATLAB. As shown in the sample response in Figure 17, the location where the second derivative equals zero and changes signs, which also corresponds to a zero slope in the first derivate is illustrated by green triangles.

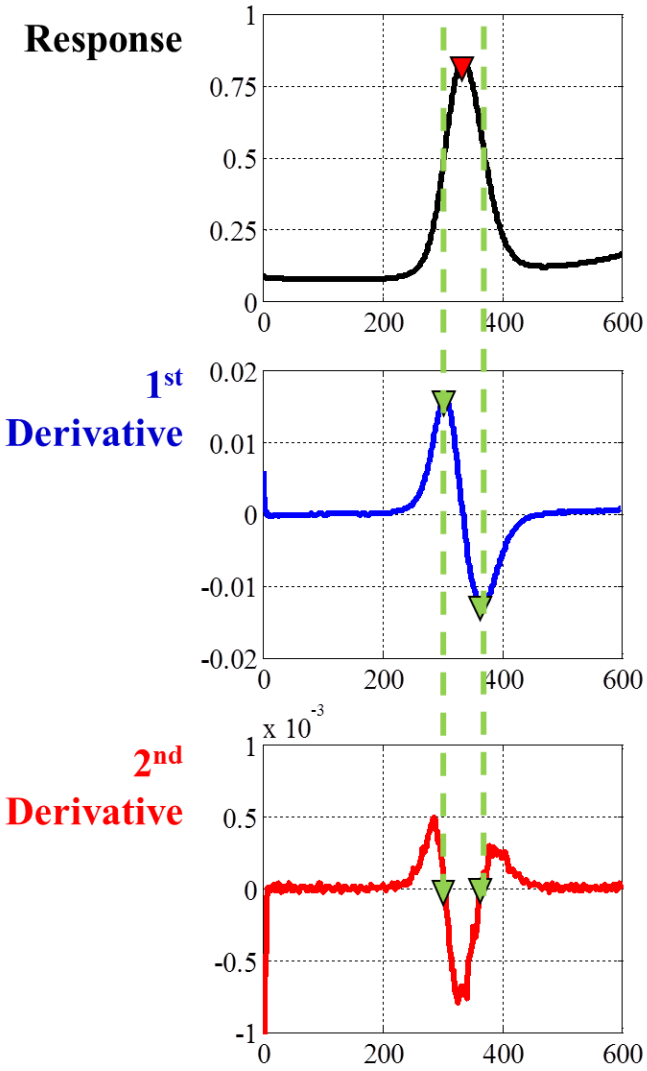

Figure 17. Sample **e**lectrochemical response and corresponding first and second derivatives showing the locations of the peak (red triangle) as well as its onset and end (green triangles).

4.2.5 Interference Characterization using the CRS

Samples of 5.6 µM CLZ alone and in mixture with individual IS from previously determined (chapter 3) were prepared at the concentration specified in Table 2, in PBS solutions. Solutions containing only the IS were also prepared in PBS as controls. These three solutions were characterized using all the sensing methods of

the CRS and their pattern was visualized using simplified heat map representations. The response patterns of each of the three samples were compared in order to elucidate the integrated responses of the mixtures and their characteristic patterns. All buffer-based tests were performed in same-day triplicates and the averages of the signals are shown graphically, such that larger positive signals correlate to larger oxidation responses.

4.2.6 Serum Characterization

Pooled commercial human serum (from human male AB plasma, originated in the USA, sterile-filtered) were divided into 1.2 mL aliquots and stored in -20 °C conditions. The frozen serum aliquots were thawed at room temperature immediately before use. Centrifree Ultrafiltration Devices (#4104) were purchased from Merck Millipore Ltd and centrifuged with 1000 µL serum samples and at a centrifugal force of 2000xg for 150 minutes to remove macromolecules (>30 kg/mol), such as proteins, from the samples. 5.6 µM CLZ was spiked in the deproteinized serum sample just prior to measurement using a 10 mM concentrated stock solution with a volume up to 1% of the total volume. The pH of serum was found to be 7.45-7.70 and ~8.54 before and after molecular weight filtration, respectively. Thus, the pH was adjusted according to Table 5 by adding the necessary volume of 1 M HCl for level comparison with the buffer-based samples.

Deproteinized serum samples were tested with and without CLZ using the CRS in order to characterize the integrated multi-level pattern of CLZ and IS for comparison

with simulated solutions. Deproteinized serum was chosen for this comparison because it more closely resembles the composition and behavior expected from the simulated (buffer-based) mixtures. The addition of proteins in the sample creates a more complex environment, where surface fouling and CLZ binding are expected in addition to physical interactions. For the purpose of this study, protein interactions with the CLZ and the sensors were not taken into account. Instead, the emphasis was in determining the effect of the simultaneous presence of interfering species in serum on the CLZ measurement.

4.3 Experimental Results

The focus of the results is the measurement of CLZ in a blood serum matrix and the determination of the individual species that affect the measurement. CLZ represents a model analyte with no known biological recognition element. The discussion highlights the properties of a CRS design and a methodology for identifying and comparing IS present in a complex biological matrix.

4.3.1 Characterization of Clozapine and Interfering Species Patterns using Cross-Reactive Sensors

In this section, the CRS elements are characterized with CLZ and the IS, and it is used as an investigational tool to study the electrochemical patterns and identify possible modes of interference. First, the multi-dimensional pattern of CLZ is characterized using the CRS, by showing the individual responses of each sensing element as well as the combined multi-dimensional pattern. Then, the CRS elements

are used to characterize the patterns of UA and CySH IS individually to show the CRS elements' ability to generate differential responses, as well as in simulated mixtures with CLZ to identify the type of interference.

4.3.1.1 Clozapine (CLZ)

Sensing element A shows a well-defined CLZ oxidation I_p at a potential of 336 mV (GCE, pH 7.4), consistent with the literature [35, 36]. In comparing sensing elements A – C, where the pH varies between 6.5 and 8.0, the I_p behavior (Figure 18a) shows an increase between the interval of pH 6.5 and 7.4 and a decrease between pH 7.4 and 8.0, a trend similar to that seen by Huang et al [42]. This could be attributed to several factors. One possibility consists of changes to pH-dependent functional groups within the GCE surface that can lead to differences in attraction/repulsion forces, reaction kinetics or reaction mechanisms. An additional factor is the effect of pH on the solubility of CLZ, which is least soluble in basic pH and could have an effect on the electrochemical response of CLZ at pH 8.0 (element C). Notably, the peak response of CLZ has the largest signal at pH 7.4 (element A).

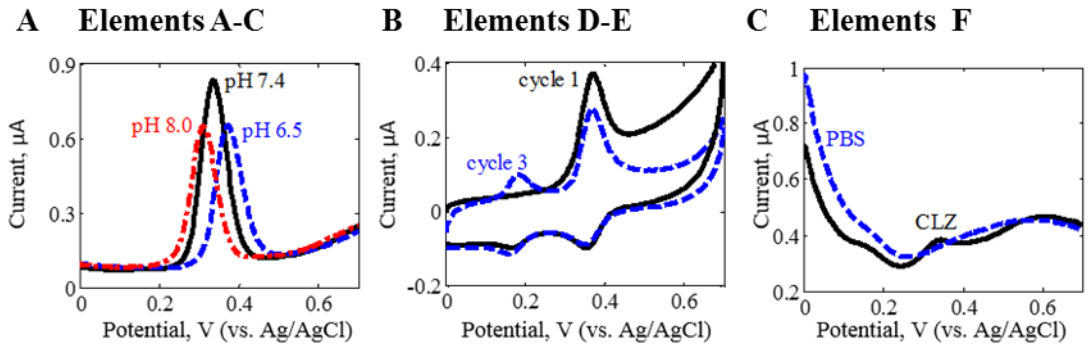

Figure 18. The CRS responses of 5.6 µM CLZ in PBS are shown across the various sensing element. (A) CLZ DPV signals at pH 6.5, 7.4 and 8.0 (elements A – C) using a GCE, (B) CLZ CV signal at pH 7.4 using GCE for cycles 1 – 3 (elements D – E), and (C) CLZ DPV signal with the Pt electrode (element F) is compared to background reactions of PBS at pH 7.4. The A – F annotations refer to the various elements in the CRS (**Table** 5). Each curve represents the average of triplicate measurements.

The behavior of the pH versus E_p follows a linear equation with a slope of 48 mV/pH and intercept value of 682 mV, as shown in Table 6. This behavior following Nernst equation demonstrates the pH dependence of the CLZ oxidation reaction. The slope value represents the ratio of protons to electrons consumed in the CLZ oxidation process and the intercept represents the potential of the CLZ reaction at standard conditions (*i.e.*, pH 0).

	Species	Peak Potential (at pH 7.4), mV	Slope, mV/pH	Intercept, mV	R^2
Individual	Clozapine	336	48	682	0.987
Species	Uric Acid	245	46	579	0.984
in PBS	L-Cysteine	347	141	1400	0.987
Mixtures	Uric Acid+Clozapine	245	47	592	0.997
in PBS	L-Cysteine+Clozapine	284	59	723	0.982

Table 6. Dependence of Dependence of peak potential on pH based on Nernst equation ($E_p = E^o - \frac{2.3RTm}{nF} pH$, equation 4), where slope values correspond to the ratio of protons to electrons consumed in the oxidation reactions and the intercept E^o is an estimate of the oxidation potential at standard conditions. The values represent the average of triplicate measurements.

Sensing elements D – E show the CLZ response when using a CV measurement technique. Figure 18b shows the oxidation and reduction peaks of the CLZ cyclic voltammogram near 340 mV as well as the appearance of additional peaks attributed to oxidation and reduction of CLZ's byproduct (as described in section 1.2.3.3) near 170 mV. Furthermore, peak variations that occur across consecutive redox cycles demonstrate a decrease of the CLZ oxidation peak and an increase of the byproduct oxidation peak, consistent with the consumption of CLZ and generation of byproduct [35]. The latter demonstrates how additional patterns can be obtained from the CV curves by accounting for the dynamic information (difference between cycles), which represents the change in redox over cycles (*i.e.*, time).

Lastly, element F shows the DPV response using a Pt electrode. As shown in Figure 18c, the Pt electrode has background peaks near 0 mV and 570 mV in the PBS solution. In the presence of CLZ, an additional DPV peak is seen at 330 mV, which is discerned from the background peaks. Due to the presence of background peaks, we suspect that changes in the sample matrix may not only affect the CLZ peak but also the background reactions. Thus, the background signal is advantageous in this type of sensor array because it can determine changes due to environmental conditions or matrix effects that may not be detectable with a GCE.

To facilitate comparison of patterns across the various sensing methods of the CRS set, a multi-dimensional heat map representation was generated as a single entity

representing the CRS patterns for the particular sample. Figure 19 illustrates a heat map that represents the set of CLZ CRS signals. The heat map shows the electrochemical current response (color scale) corresponding to the applied potential (x-axis), for each sensing element of the CRS (y-axis). The pattern of CLZ across the CRS elements, shown in Figure 19a, represents a visualization tool, which transforms the same electrochemical responses (from Figure 18a-c) into a convenient one-entity representation. Furthermore, Figure 19b represents a simplified heat map, which only shows the peak widths and locations across the CRS elements, which are the most important parameters for differentiating various species. The latter provides a more robust method of comparing and matching patterns across various samples.

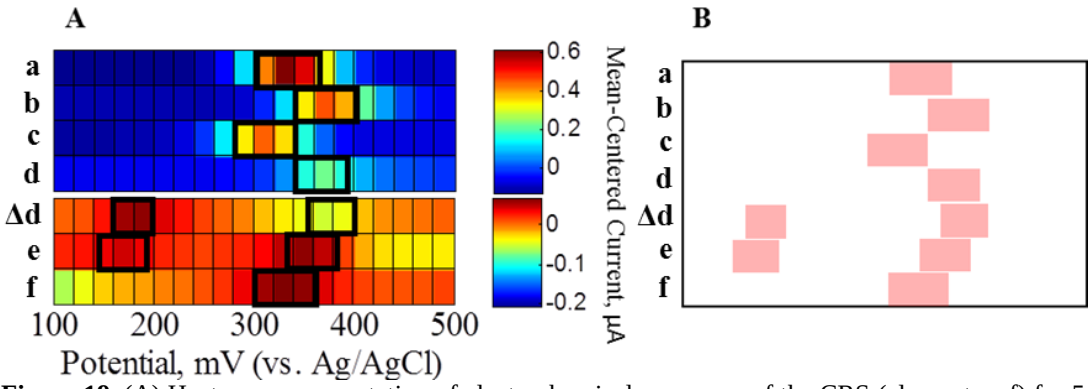

Figure 19. (A) Heat map representation of electrochemical responses of the CRS (elements a-f) for 5.6 μM CLZ tested individually in PBS buffer. Each row represents a different element (A-F) from **Table** 5. Black outlines represent the location of peaks in the signal. Each response represents the average absolute value of triplicate measurements. (B) Simplified heat map highlighting only the locations and peak widths corresponding to the black outlines in A.

4.3.1.2 Uric Acid (UA)

UA has a characteristic oxidation peak at 245 mV in pH 7.4 buffer (GCE, element A) as shown in Figure 20a. Elements A – C illustrate how UA's peak potential shifts with varying pH (Figure 20a). Upon fitting to the Nernst equation, a slope value of 46

mV/pH was found to be similar to that of CLZ (48 mV/pH), elucidating that the same ratio of protons to electrons were involved in the oxidation reactions of UA and CLZ (Table 6). Nonetheless, the intercept value of 579 mV, representative of the E^o, provides a distinguishable parameter between the two species. In relation to interference in the CLZ measurement, a lower UA response would be preferred in order to decrease the potential overlap of the CLZ and UA peak signals. The highest UA response is seen at pH 6.5 (element B) and the lowest at pH 8.0 (element C).

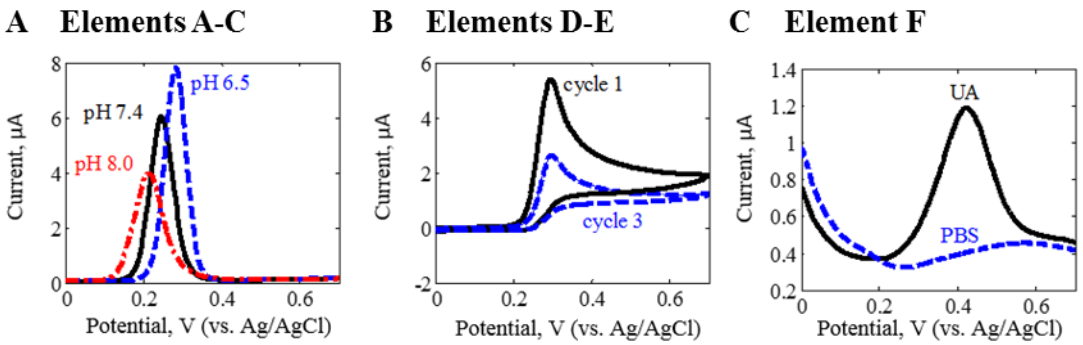

Figure 20. The CRS responses of 410 µM UA in PBS are shown across the various sensing element. (A) UA DPV signals at pH 6.5, 7.4 and 8.0 (elements A – C) using a GCE, (B) UA CV signal at pH 7.4 using GCE for cycles 1 – 3 (elements D – E), and (C) UA DPV signal with the Pt electrode (element F) is compared to background reactions of PBS at pH 7.4. The A – F annotations refer to the various elements in the CRS (**Table** 5). Each curve represents the average of triplicate measurements.

When CLZ was measured in the presence of UA in PBS, the patterns obtained throughout the CRS were similar to those seen for UA-only solutions, as illustrated in the heat map in Figure 21b. For instance, element A shows a single DPV oxidation for the UA/CLZ mixture peak positioned at the characteristic UA location. It is reasonable to assume that the CLZ peak current may be masked by the UA response, which is 5-fold higher in amplitude than the CLZ peak response and 73-fold higher in concentration. Similarly, the pH trend shown in Table 6 closely matches the UA

trend. This finding corresponds with previous studies, where interference from high concentrations of UA for electrochemical CLZ measurements was reported [42].

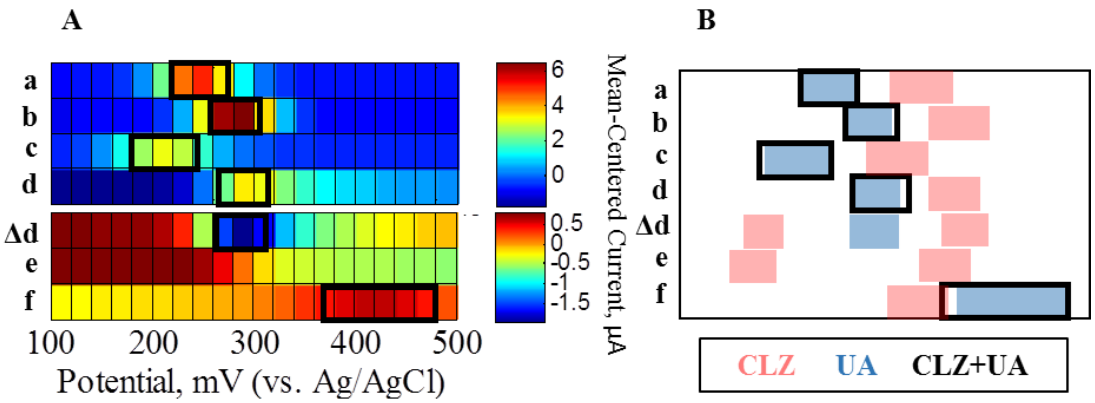

Figure 21. (A) Heat map representation of electrochemical responses of the CRS (elements a-f) for 410 µM UA tested individually. Black outlines represent the location of peaks. (B) Simplified heat map showing the electrochemical peak locations of 410 µM UA tested individually in mixture with 5.6 µM CLZ, as well as control 5.6 µM CLZ tested individually for comparison, in PBS buffer. Each response represents the average absolute value of triplicate measurements. Each heat map contains an individual color scale.

Sensing elements D – E show the UA response using a CV technique. The CV oxidation peak potential of UA is positioned at 300 mV, as seen in Figure 20b. This peak decreases with cycles (element ΔD), as seen by the dark blue area positioned near 300 mV in the heat map representation (Figure 21). This behavior suggests a large consumption of UA throughout cycling, likely due to the irreversible redox nature of this species, which is also seen by the lack of reduction peaks in element E. Interestingly, in the presence of CLZ, the CV reduction peak of CLZ was masked in the presence of UA. The masking of CLZ oxidation and reduction peaks suggest that UA may be preventing CLZ reduction at the electrode surface, which may be caused UA's potent antioxidant activity. Another suggestion may be the formation of linkages between oxidized UA and the GCE surface due to the presence of high

concentration secondary amines in UA, which can foul the electrode surface and thus decrease the current response of CLZ after UA is oxidized [95, 96].

Lastly, element F shows the response of UA using a Pt electrode. As seen in Figure 20c, UA shows a drastic shift of 180 mV in its E_p position, compared to the GCE, at the Pt electrode. Because CLZ did not show similar E_p shifting behavior, the relative E_p position of CLZ to UA can act as a parameter that varies depending on the electrode material. This can provide an additional characteristic signal for the CLZ pattern in the presence UA. Nonetheless, the larger width of the UA signal at the Pt electrode (compared to the GCE) overlaps with the position of the CLZ peak. In simulated mixtures solutions containing CLZ and UA, only one peak potential is seen, as shown in Figure 21b (element F).

Even when the CLZ peak appears to be masked by the upper UA concentration in the simulated mixtures, (serum) complex samples may have different integrated responses in the simultaneous presence of other species. This is further studied in section 4.3.2.

4.3.1.3 L-Cysteine (CySH)

CySH has a wide characteristic oxidation peak at 347 mV in pH 7.4 buffer (GCE, element A) as shown in Figure 22a. This peak is suggested to correspond to a 2-step reaction of CySH's thiol group, which yields CyS^{-1} and subsequently disulfide CyS-SCy [100, 101]. The disulfide bond formation is analogous to the mechanism of

disulfide bond formation between polypeptide chains during protein folding processes in the body, where CySH serves a critical role [100]. Elements A – C illustrate how the peak potential shifts with varying pH. Upon fitting to the Nernst equation (Table 6), a slope value of 141 mV/pH and an intercept of 1400 mV differed from those found for CLZ or UA. This suggests characteristic differences in electrochemical processes among these species, with much higher proton to electron ratio and E^o values for CySH. Additionally, large differences in the I_p values of CySH were seen across varying pH, with a distinguishable wide peak observed at neutral pH, which decreases at pH 8.0 and becomes ill-defined at pH 6.5. Since CLZ has an E_p position similar to that of CySH, the least amount of overlap between the CLZ and CySH peaks is presumed to occur at pH 6.5, where the CySH response is lowest.

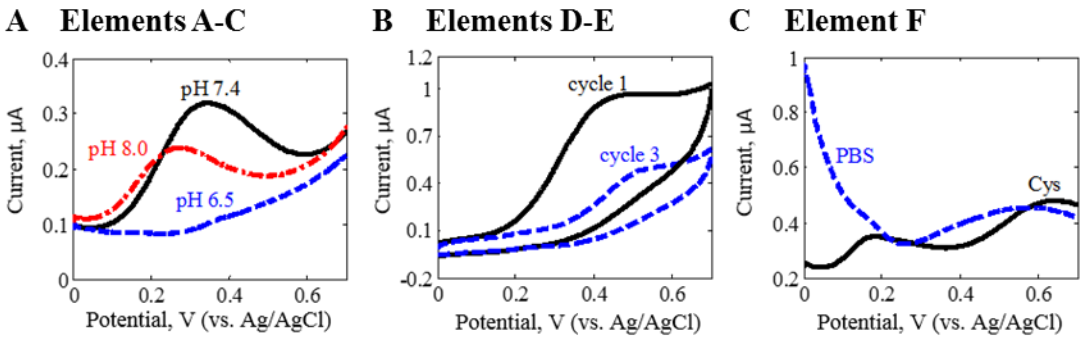

Figure 22. The CRS responses of 60 µM CySH in PBS are shown across the various sensing element. (A) CySH DPV signals at pH 6.5, 7.4 and 8.0 (elements A – C) using a GCE, (B) CySH CV signal at pH 7.4 using GCE for cycles 1 – 3 (elements D – E), and (C) CySH DPV signal with the Pt electrode (element F) is compared to background reactions of PBS at pH 7.4. The A – F annotations refer to the various elements in the CRS (Table 5). Each curve represents the average of triplicate measurements.

As can be seen in Figure 23, the response of the CLZ/CySH simulated mixture in pH 7.4 buffer (GCE, element A) contains one major peak near 284 mV, with a 0.62-fold change in I_p compared to that of CLZ individually. In parallel, an additional smaller

peak near 472 mV appears in the response of the simulated mixture. Since this peak is not observed in either CLZ or CySH individual responses, a cross-reaction between these two components is likely, which can also explain the shifted E_p and decreased I_p. Corroborating this suggestion, Van Leeuwen et al. showed that the CySH-containing glutathione species can react with activated CLZ to form CyS-CLZ adducts, which are electroactive at higher potentials [35]. Thus, the latter peak shown at 472 mV may be the electroactive product of the Cys-CLZ cross-reaction. Moreover, the pH dependency of the major peak of the CLZ/CySH mixture near 284 mV (at pH 7.4, GCE, element A) follows a trend with varying pH shown in Table 6, with a slope (59 mV/pH) and intercept (723 mV) values closer to those of CLZ (48 mV/pH and 682 mV, respectively) than to the slope and intercept values of CySH (141 mV/pH and 1400 mV). Thus, this peak is likely governed by the CLZ rather than the CySH reaction kinetics. The additional peak near 472 mV also has a pH-dependent slope (43 mV/pH) closely resembling that of CLZ as well.

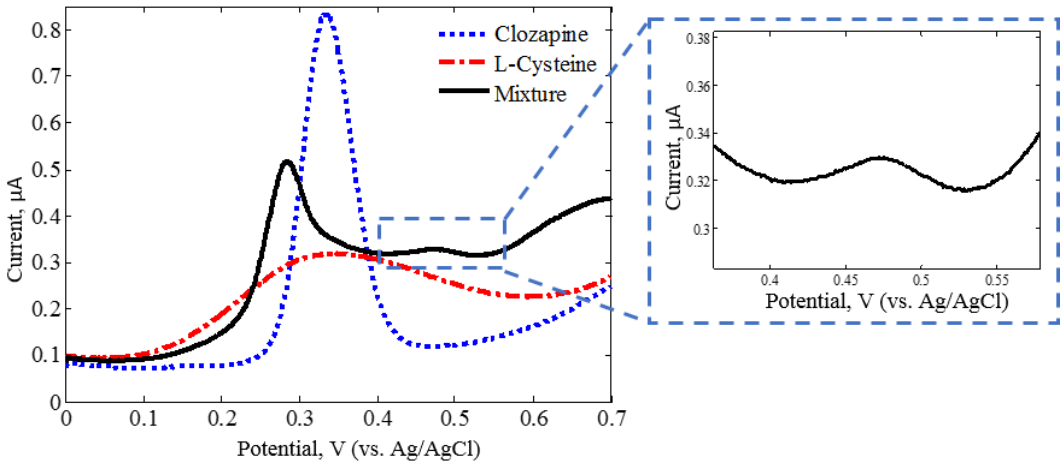

Figure 23. Differential pulse voltammetry (DPV) of 5.6 µM CLZ, 60 µM CySH, and their mixture in PBS (pH 7.4) at the glassy carbon electrode (element A). This figure demonstrates the additional peaks generated by the cross-reaction of CLZ and CySH. Signal response represents an average of triplicate measurements.

Sensing elements D – E show the CySH response using a CV technique. The CySH CV oxidation peak (element D) is seen as a wide peak near 480 mV (Figure 22b), whose magnitude decreases. This behavior together with the lack of a reduction peak suggests consumption of CySH at the electrode, since the oxidized species was not regenerated. Additionally, the increase in the E_p location with cycling suggests possible fouling of the electrode surface. Lastly, the reduction peak of CLZ is masked in the presence of CySH as seen in the heat map (element E) of Figure 24b, likely due to the hypothesized CLZ/CySH cross-reaction, which would increase the consumption of CLZ before it can be reduced back.

Lastly, element F shows the response of CySH using a Pt electrode. As seen in Figure 22c, the CySH oxidation peak at the Pt electrode is positioned close to that seen with GCE, with a 70 mV shift to higher $E_{p.}$ Moreover, an additional peak appears near 0.15 V, but no conclusions can be drawn about this peak since the responses between 0 and 200 mV also correspond to background oxidation processes as seen by the PBS response for element F (Figure 22c). In the simulated mixture of CySH and CLZ, the Pt electrode illustrates a pattern that masks both CySH and CLZ peaks as seen in Figure 24b.

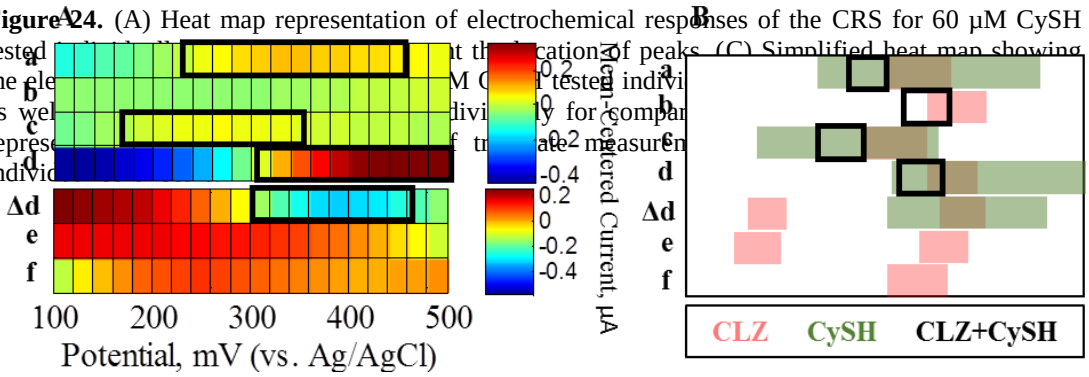

Figure 24. (A) Heat map representation of electrochemical responses of the CRS for 60 µM CySH tested [illegible] at the location of peaks. (C) Simplified heat map showing the ele[illegible]M C[illegible] tested individ[illegible] as wel[illegible]divi[illegible]ly for compar[illegible] repres[illegible]f tr[illegible]ate measurem[illegible] individ[illegible]

4.3.2 Matching Individual Species Patterns to Complex Serum Patterns

4.3.2.1 Serum Measurement using a Single Sensor

The electrochemical activity of un-spiked and CLZ-spiked (deproteinized) serum at pH 7.4 was tested with a single GCE sensor using the DPV technique, corresponding to element A from the CRS. Figure 25 shows the voltammograms and corresponding heat map representing the response of serum with and without the addition of CLZ. A predominant peak present in the DPV response of the serum background was observed at 248 mV and another smaller amplitude peak at 647 mV. Comparing these patterns with the corresponding buffer-based patterns, the first peak can be matched to the characteristic oxidation potential of UA (245 mV). While about 6 – 8 times higher I_p magnitudes were expected for the UA signal due to its high physiological concentrations, species degradation may have occurred during sample preparation, transportation and preservation that may account for the decreased response [102, 103]. A second peak of the serum background occurred at 647 mV, and this did not match any of the interfering species tested in the screening study. This may be a result of integrated signal changes in the simultaneous presence of several interfering species or a result of species (endogenous or exogenous) not assessed in this study. Lastly, current peaks that can be matched to the CySH peak pattern were not observed. This species may not be detectable in serum due to its low concentrations, overlapping with the larger UA peak, or potentially interacting (*i.e.*, cross-reactions) with other serum components during storage and handling.

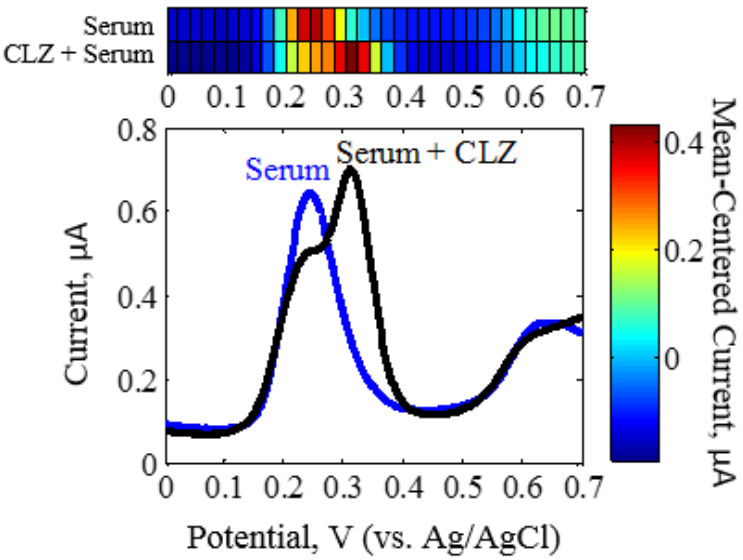

Figure 25. Differential pulse voltammetry (DPV) of serum with and without 5.6 µM CLZ using sensing element A, and corresponding heat map pattern representation. All solutions were tested using GCE, and represent an average of duplicate measurements.

In the presence of CLZ in the serum sample, a third peak at 312 mV appears in the DPV response (Figure 25). This peak is near the location of the CLZ peak measured in buffer and has about a 0.78-fold decreased I_p compared to the buffer-based response. Furthermore, the same peaks found in the un-spiked serum response remained present in the spiked serum response, with a slight decrease of the suspected UA peak. This decrease may be due to the cross-reactive dependencies between CLZ and UA.

4.3.2.2 Serum Measurement using the Multi-Dimensional CRS

To further match the electrochemical response of un-spiked and CLZ-spiked serum, the CRS was utilized. The multi-dimensional tool can aid in validating the species that correspond with the observed patterns, by discerning and matching patterns across the set of sensors, for tests carried out on interfering species and simulated mixtures.

pH Changes. Elements A – C illustrate the change in serum electrochemistry with varying pH at the GCE, as shown in Figure 26a. In the un-spiked serum, the suspected UA peak (at 248 mV, element A) follows a pH response trend (Table 7) matching that of the individual UA. Thus, this result further points to the likelihood of this peak representing the UA oxidation since the fitted values corresponding to the slope (proton to electron production ratio) and intercept (standard potential) of the Nernst equation are similar to that of UA oxidation. Similarly to the UA buffer-based trend, the lowest response for the primary serum peak is observed for pH 6.5, which may represent a condition of maximal signal-to-noise ratio for the CLZ measurement.

Figure 26. The CRS responses of deproteinized serum are shown across the various sensing element. (A) Serum DPV signals at pH 6.5, 7.4 and 8.0 (elements A – C) using a GCE, (B) serum CV signal at pH 7.4 using GCE for cycles 1 – 3 (elements D – E), and (C) serum DPV signal with the Pt electrode (element F) is compared to background reactions of PBS at pH 7.4. (D) CLZ-spiked serum DPV signals at pH 6.5, 7.4 and 8.0 (elements A – C) using a GCE, (E) CLZ-spiked serum CV signal at pH 7.4 using GCE for cycles 1 – 3 (elements D – E), and (E) CLZ-spiked serum DPV signal with the Pt electrode (element F) is compared to background reactions of serum at pH 7.4. The A – F annotations refer to the various elements in the CRS (Table 5), and the proteins were removed from serum samples. Each curve represents the average of duplicate measurements.

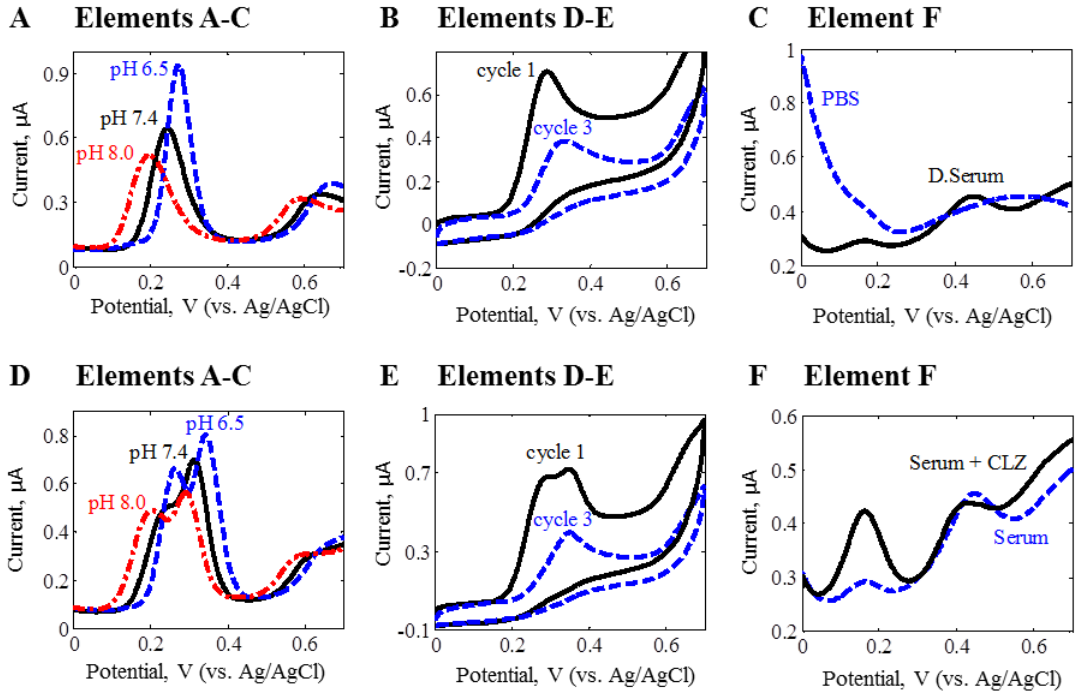

Interestingly, the Nernst equation pH versus E_p fitting for the CLZ-spiked serum shows a consistent decrease in slope and intercept values of the two major peaks (suspected-UA and CLZ) compared to the buffer-based results, as shown in Table 7. This discrepancy in the pH trends may be caused by cross-reactions between UA and CLZ in the presence of other interfering species in this complex mixture, and further illustrates the dependence of the analyte measurement on other components of the sample. The comparison between un-spiked and CLZ-spiked serum responses at varying pH is illustrated in Figure 27. Notably, the highest resolution and differentiation of the two major peaks as well as the higher CLZ signal is seen at pH 8.0 (element C). In contrast, buffer-based CLZ response obtained the largest peak at pH 7.4, which raises another difference between buffer and serum based samples that elucidates changes in the analyte signal of the integrated and complex behavior of blood serum.

	Species	Peak Potential (at pH 7.4), V	Slope, V/pH	Intercept, V	R^2
Un-Spiked Deproteinized Serum	Uric Acid (suspected)	0.248	0.051	0.610	0.894
CLZ-Spiked Deproteinized Serum	Clozapine	0.312	0.0349	0.569	0.997
	Uric Acid (suspected)	0.248	0.0367	0.5063	0.860

Table 7. Dependence of Dependence of peak potential on pH based on Nernst equation ($E_p = E^o - \frac{2.3RTm}{nF} pH$, equation 4), where slope values correspond to the ratio of protons to electrons involved in oxidation reactions and the intercept E^o is an estimate of the oxidation potential at standard conditions. Triplicate measurements were carried out for PBS-based solutions and duplicate measurements for serum-based solutions.

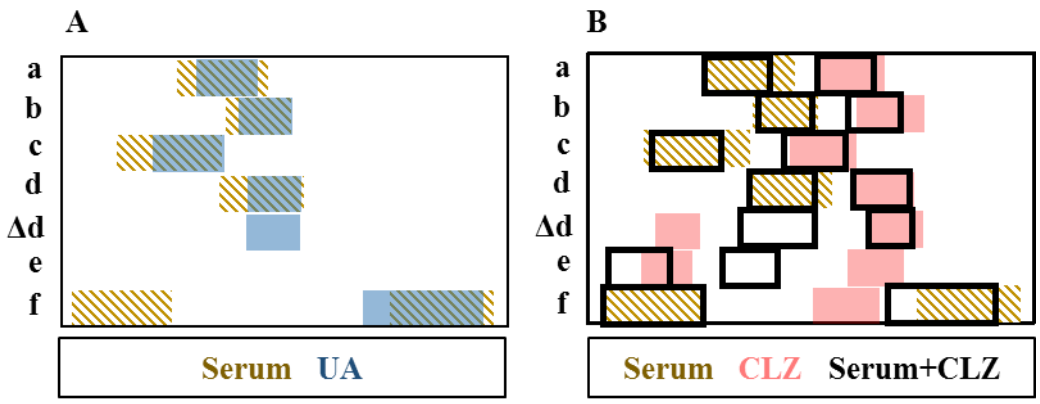

Figure 27. Simplified heat map representation of electrochemical responses of the CRS elements (a-f) of (A) serum compared to UA individually in PBS buffer, showing the matches in their patterns, and of (B) serum before and after CLZ-spiking compared to the expected individual CLZ patterns, showing the matches in their patterns.

CV Technique. Elements D – E illustrate the CV responses and include element ΔD, which represents the difference in current over a period of three CV cycles (or time). As seen in Figure 27a, the CV oxidation (element D) response is similar to the DPV response (element A). No discernable changes in the CV response over cycles (dynamic information, element ΔD) or reduction peak (element E) were seen in serum (Figure 27a). However, once CLZ was spiked into serum, CLZ peaks corresponding to elements ΔD and E appeared, as seen in Figure 27b. Thus, these two elements may be representative of UA-independent serum responses.

Platinum Electrode. Element F corresponds to the Pt electrode response. As seen in Figure 26c, a major peak near 430 mV was observed for the un-spiked serum sample. The peak location is drastically different compared to the background peak observed at the GCE (element A). This peak shift across the two electrodes matched the behavior seen for the individual UA buffer-based response (Figure 27b), further corroborating this peak likely corresponds to UA. A difference in the current response

of PBS compared to that of serum in the range of 0 – 200 mV was observed. This behavior matches the behavior seen for CySH, although since a background response of the PBS background occurs in the same potential range, no measurements in this region can be directly assigned to one particular species.

When CLZ was spiked into serum, no additional peaks were seen compared to un-spiked serum. This sensing element suffers from reduced resolution compared to the GCE; however, it shows a characteristic signal of the UA species.

4.3.2.3 Performance of Serum-Based Sensing

Figure 28a demonstrates the increasing current response of the suspected-UA peak with increasing UA spiking, which provides further evidence that the background serum peak is indeed UA. Furthermore, this plot is representative of the UA variability that would likely occur from person to person. Figure 28b shows the increasing current response of the CLZ peak with increasing CLZ spiking, which can be seen to be convoluted with the UA peak, although a CLZ concentration dependency is observed.

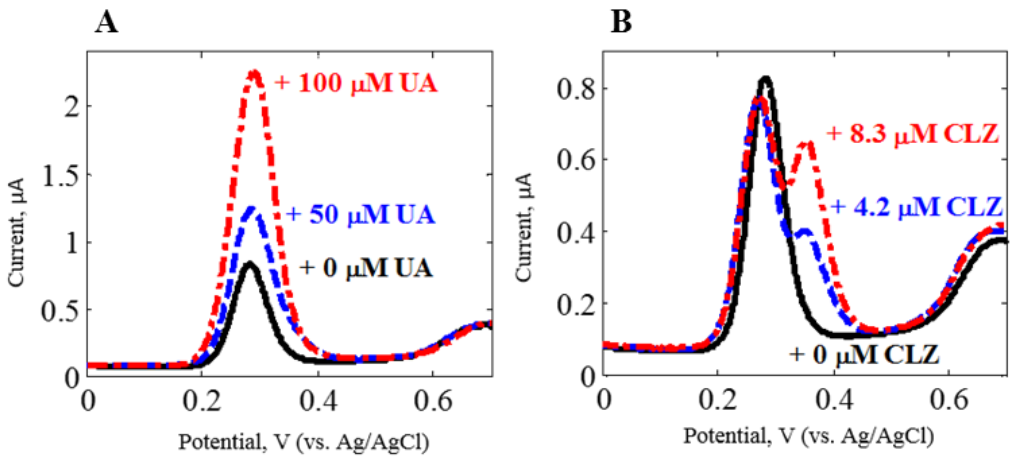

Figure 28. Concentration dependent variation for serum spiked with (A) UA at 0, 50 and 100 µM and (B) CLZ at 0, 4.2 and 8.3 µM.

Due to the proximity of the UA and CLZ peaks, variability in the dominant UA peak will cause variability in the CLZ peak such that the CLZ measurement is dependent on the UA concentration in the given sample. As seen in Figure 29for varying UA background levels, the sensitivity of the CLZ calibration varies, with a 1.67-fold decrease in sensitivity (*i.e.*, slope) upon increasing the UA concentration by 50 µM.

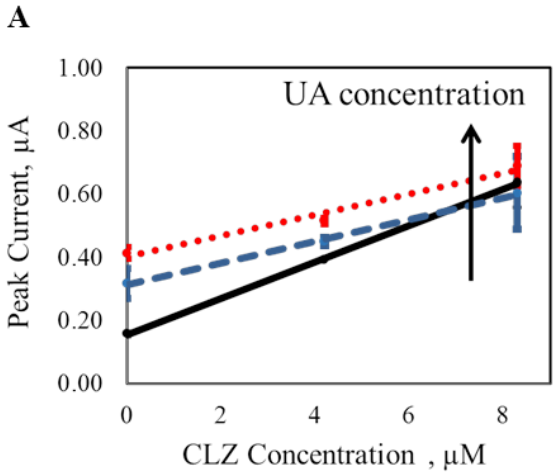

B

	Slope	Intercept
+0 µM UA	0.058	0.154
+50 µM UA	0.035	0.312
+ 100 µM UA	0.033	0.400

Figure 29. (A) CLZ calibration in serum at varying levels of UA spiked into the sample to account for population variability. Serum was spiked with 0 (black), 50 (blue) and 100 (red) µM UA. (B) The linear fit is represented by the slope and intercept values of each CLZ calibration at various UA concentrations.

4.4 Summary

A set of 7 CRS were utilized to characterize the interaction of UA and CySH with CLZ and how their integrated responses in serum affect the CLZ measurement. UA appears to mask the CLZ peak response in buffer due its high concentration and the close proximity of its characteristic peak to that of CLZ. Additionally, UA's antioxidant properties may prevent CLZ oxidation at the surface. CySH, on the other hand, showed evidence of cross-reactions with CLZ, with the detection of an electroactive byproduct. The presence of CySH appeared to shift the CLZ peak to lower potentials and decrease its peak amplitude. By understanding the pattern of CLZ in the presence of each interfering species, one can begin to understand how the CLZ response is affected by the simultaneous presence of other species.

Heat map representations of the multi-dimensional responses were used to facilitate visual comparison among the various species. Importantly, the multiple dimensions of the CRS allow for comparison of characteristic patterns at 7 differential elements, which increases the certainty of the evaluation. Upon applying the CRS to serum samples, UA and CLZ patterns were matched to individual species responses across the elements of the CRS. The CySH pattern was not discerned in serum, likely due to a matrix effect such as the simultaneous presence of other species in solution that can affect the oxidation and degradation of this lower concentration antioxidant. Some differences in the patterns of UA and CLZ in buffer and in blood serum were observed and attributed mainly to integrated matrix effects and additional molecular

cross-reactivity. These results further highlight the challenges of inter-dependence between the analyte and other serum components in POC blood tests, in this case between CLZ and UA. Nonetheless, the results demonstrate that collecting broader information enabled discerning of patterns in simulated and complex serum matrix. Furthermore, information about the specific species responsible for the major interference in the CLZ measurement can help in designing sensors as well as sample preparation protocols (*i.e.*, separations, chemical treatment) that are targeted toward this limitation.

Chapter 5: Conclusion and Future Work

5.1 Conclusion

This thesis described the analysis of endogenous interference in blood-based sensors using electrochemical measurements. Specifically, interference in a therapeutic drug monitoring sensor for CLZ antipsychotic was evaluated with the goal of identifying major interfering species present in the blood sample and suggesting targeted sensor design guidelines accordingly. First, the selectivity properties of a previously-used ccRCS modified sensor was qualified. The ccRCS demonstrated semi-selectivity properties for CLZ compared to other interfering species. However, other interfering species present in blood affected the ccRCS CLZ measurement.

To understand which species affect the CLZ measurement in blood serum, a broader and more comprehensive methodology for studying interferences was developed. This method compared studies of individual species with studies of the complex blood serum matrix, where all species are present simultaneously. An initial coarse screening was followed by the use of a novel set of CRS for characterizing response patterns across the different sensors. The CRS response was shown to produce differential responses with the capability of providing synergistic chemical information and providing multi-dimensional patterns for sample comparison. By mapping the CRS responses onto multi-dimensional heat maps, characteristic patterns were compared between buffer and serum samples to discern and match patterns across the matrices. This study demonstrated the identification of the major

interfering species for CLZ sensing using blood serum samples. Furthermore, the interdependence between CLZ and other serum components (in this case, uric acid) in POC blood tests was highlighted. This information can aid in designing sensors as well as sample preparation protocols (*i.e.*, separations, chemical treatment) that can improve the reliability and selectivity of the device. Lastly, this method can be applied to the other electrochemical CLZ sensor materials by performing an abbreviated screening test using specific sensor design with simulated mixtures containing the electroactive species shown in Table 2. This screening method has broader impact because it provides a systematic process that can be applied to any sensor/analyte, with minor changes to the selection of interfering species of similar sensors.

5.2 Future Work

5.2.1 Exogenous Interfering Species Characterization

In this study, species naturally present (endogenous) in serum were studied because they make up the average composition of blood in the population. Thus, samples of pooled serum represent this average composition and can be acquired commercially. On the other hand, the presence of exogenous (external species such as medications) species increases the complexity of serum and introduces additional potentially interfering species to the sample. Thus, the interference identification methodology shown in this thesis can be expanded to include exogenous species, and the developed CRS tool can be similarly applied to identify interfering exogenous species. Exogenous species with the potential to interfere with CLZ will be similarly

identified from the common mediations used by the schizophrenia population of interest as well as those most commonly used by the general population, narrowed down based on abundance and likelihood of interference and coarse screening, and characterized using the CRS method shown here. The integrated understanding of endogenous and exogenous species in serum and their effect on the CLZ measurement elucidates the total expected interference in real samples of schizophrenia subjects, which is useful for appropriate sensor design that accounts for differences in the serum composition among patients.

5.2.2 Microsystem Device Integration

Translation of the CRS into a POC microfluidic system will ultimately enable real-time treatment management in schizophrenia. This integrated system will also enable high-throughput testing of various serum samples. For instance, testing serum samples where the CLZ and UA concentrations are simultaneously varied across the expected physiological concentrations can be used for training chemometric models to take UA interference into account. Similarly, testing various schizophrenia patients taking CLZ with and without other medications can be used for training chemometric models. The high-throughput provided by microfluidic devices will allow for testing the large number of samples required for chemometric models. Furthermore, integrating material modifications, such as the carbon nanotubes will improve the sensitivity and lower the limit of detection of CLZ in order to achieve detection the entire CLZ physiological concentration range.

5.2.3 Multivariate Chemometric Model Integration

The ultimate sensor design is envisioned as an integrated CRS platform incorporated with savvy pattern recognition (*i.e.*, chemometric) data processing that takes to account the measurement inter-dependence between components in serum-based sensors. For instance, concepts such as the electronic tongue, which has enabled multi-analyte assessment in complex mixtures by coupling multi-sensor responses with pattern recognition (*i.e.*, chemometric) models, can be an appropriate platform [66, 104-108]. This method relies on CRS that each provide diverse and synergistic information regarding the markers of interest as well as other variable background signals, creating fingerprint patterns for the markers of interest. Quantitative or qualitative models can be applied to obtain either presence/absence information or concentration values [66]. Moreover, advanced models such as artificial neural networks are capable of being trained to a certain sample matrix, such as the particular baseline signal of an individual's serum, and can account for the sample matrix changes that may differ from person to person [67]. Thus, the diversity of a sensor array provides a multi-dimensional tool that can account for variable component in blood.

The CRS demonstrated here was designed of multiple CRS, similar to the electronic tongue platforms, and it can be directly used in the application of chemometric modeling. By training a chemometric model with varying concentrations of CLZ and interfering species in serum across the CRS, an integrated and quantitative analysis tool for CLZ in serum can be developed. Such a platform would account for varying

levels of serum composition (including varying UA levels) in the prediction of CLZ, thereby increasing the certainty of the measurement and improving the selectivity of the sensor system.

5.2.4 Protein Binding/Unbinding

Because many drugs become highly bound to protein upon entering in the circulation, techniques for unbinding protein-bound drugs prior to measurement have the potential for increasing the sensitivity of the sensor. For instance, CLZ mainly binds to alpha-1-glycoprotein (AAG) and also binds to albumin (HSA) in blood, with a portion that remains free in solution. A study of the ability of electrochemical techniques to sense protein-bound CLZ and of various unbinding methods to free the protein-bound CLZ portions is proposed. For instance, CLZ can be incubated with proteins and filtered using a size-exclusion membrane such that only the protein-bound CLZ portion can be separated and tested for electrochemical activity. Next, several unbinding techniques such as changing temperature or pH, or catalytically cleaving the proteins can be applied to protein-bound CLZ and characterized.

5.2.5 Identification of Biomarkers

The CRS can be additionally used as an investigational tool to compare serum samples across varying populations to serve in the identification of potentially useful biomarkers. For instance, one can imagine a reverse application of the methodology shown in this work whereby serum samples from a specific population are compared

to samples from healthy subjects using the CRS. By comparing the CRS patterns between these populations, discovery of differences among the populations and comparison to a buffer-based database of individual component signals can lead to identification of those differences. This can provide insights not only about potential species that can serve as biomarkers in the sample population of interest, but also regarding broader responses (of multiple species simultaneously) which can serve as an integrated biomarker pattern. Thus, pattern differences between the populations shown by the CRS can elucidate the presence of potential individual or combined biomarker patterns, which can eventually be further characterized and identified.

Glossary

POC = point-of-care

TDM = therapeutic drug monitoring

CLZ = clozapine

CV = cyclic voltammetry

DPV = differential pulse voltammetry

RCS = redox cycling system

ccRCS = chitosan-catechol RCS

Ru = hexaammineruthenium

Fc = ferrocene dimethanol

CRS = cross-reactive sensors

UA = uric acid

CySH = L-cysteine

Bibliography

1. Olesen, O.V., *Therapeutic drug monitoring of clozapine treatment.* Clin Pharmacokinet, 1998. **34**(6): p. 497-502.
2. Buur-Rasmussen, B. and K. Brosen, *Cytochrome P450 and therapeutic drug monitoring with respect to clozapine.* European Neuropsychopharmacology, 1999. **9**(6): p. 453-459.
3. Gubala, V., et al., *Point of care diagnostics: status and future.* Anal Chem, 2011. **84**(Fundamentals and Applied Reviews in Analytical Chemistry): p. 487-515.
4. Price, C.P., *Regular review: point of care testing.* BMJ, 2001. **322**(7297): p. 1285-1288.
5. St. Louis, P., *Status of point-of-care testing: promise, realities, and possibilities.* Clin Biochem, 2000. **33**(6): p. 427-440.
6. Blum, L.J. and P.R. Coulet, *Biosensor Principles and Applications*1991: Carcel Dekker, Inc.
7. Mello, L.D. and L.T. Kubota, *Review of the use of biosensors as analytical tools in the food and drink industries.* Food Chem, 2002. **77**(2): p. 237-256.
8. de Souza Gil, E. and G. Rodriguez de Melo, *Electrochemical biosensors in pharmaceutical analysis.* Brazilian J of Pharm Sci, 2010. **46**(3): p. 375-391.
9. Toghill, K.E. and R.G. Compton, *Electrochemical non-enzymatic glucose sensors: a perspective and an evaluation.* Int J Electrochem Sci, 2010. **5**(9): p. 1246-1301.
10. Institute, C.a.L.S., *Interference testing in clinical chemistry: approved guideline- second edition*, 2005: Pennsylvania, US.
11. von Lode, P., *Point-of-care immunotesting: approaching the analytical performance of central laboratory methods.* Clin Biochem 2005. **38**(7): p. 591-606.
12. Schleicher, E., *The clinical chemistry laboratory: current status, problems and diagnostic prospects.* Anal Bioanal Chem, 2006. **384**: p. 124-131.
13. Yoo, E. and S. Lee, *Glucose biosensors: an overview of use in clinical practice.* Sensors (Basel), 2010. **10**(5): p. 4558-4576.
14. Park, S., H. Boo, and T. Dong Chung, *Electrochemical non-enzymatic glucose sensors.* Anal Chim Acta, 2006. **556**(1): p. 46-57.
15. Goyal, R.N., V.K. Gupta, and S. Chatterjee, *Voltammetric biosensor for the determination of paracetamol at carbon nanotube modified pyrolytic graphite electrode.* Sens Act B: Chem, 2010. **149**(1): p. 252-258.
16. Arslan, F., *An amperometric biosensor for uric acid determination prepared from uricase immobilized in polyaniline-polypyrrole film.* Sensors, 2008. **8**(9): p. 5492-5500.
17. Hiemke, C., et al., *AGNP consensus guidelines for therapeutic drug monitoring in psychiatry: update 2011.* Pharmacopsychiatry, 2011. **44**: p. 195-235.

18. Jennison, T.A., et al., *A rapid gas chromatographic method quantitating clozapine in human plasma or serum for the purpose of therapeutic monitoring.* J Anal Toxicol, 1995. **19**(7): p. 537-541.
19. Jefferson, J.W., *Finger-stick lithium test: in-office alternative to laboratory-based methods.* Current Psychiatry, 2005. **4**(10): p. 111-117.
20. Freeman, D.J. and L.K. Oyewumi, *Will routine therapeutic monitoring have a place in clozapine therapy?* Clin Pharmacokinet, 1997. **32**(2): p. 93-100.
21. Ben-Yoav, H., et al., *Redox cycling- based amplifying electrochemical sensor for in situ clozapine antipsychotic treatment monitoring.* Electrochim Acta, 2014. **130**(1): p. 497-503.
22. Winkler, T.E., et al. *Microsystem for particle counting and sizing with tunable sensitivity and throughput*. in *Hilton Head Workshop 2014: A Solid-State Sensors, Actuators and Microsystems Workshop*. 2014. Hilton Head, SC, USA.
23. Kelly, D.L., et al. *Development of a lab-on-a-chip biosensor for clozapine monitoring*. in *ACNP 52nd Annual Meeting*. 2013. Hollywood, FL, USA.
24. Ozkan, S.A., B. Uslu, and A.H. Aboul-Enein, *Analysis of pharmaceuticals and biological fluids using modern electroanalytical techniques.* Crit Rev Anal Chem, 2003. **33**(3): p. 155-181.
25. Uslu, B. and S.A. Ozkan, *Electroanalytical Application of Carbon Based Electrodes to the Pharmaceuticals.* Anal Lett, 2014. **40**(5): p. 817-853.
26. Jacobs, C.B., M.J. Peairs, and B.J. Venton, *Review: Carbon nanotube based electrochemical sensors for biomolecules.* Anal Chim Acta, 2010. **662**: p. 105-127.
27. Belding, S.R., et al., *Nanoparticle-modified electrodes.* Phys Chem Chem Phys, 2010. **12**: p. 11208-11221.
28. Zen, J.-M., A.S. Kumar, and D.-M. Tsai, *Recent updates of chemically modified electrodes in analytical chemistry.* Electroanal, 2003. **15**(13): p. 1073-1087.
29. Mohajeri, S.A., G. Karimi, and M.R. Khansari, *Clozapine imprinted polymers: Synthesis, characterization and application for drug assay in human serum.* Anal Chim Acta, 2010. **683**: p. 143-148.
30. Rahman, M.A., et al., *Electrochemical sensors based on organic conjugated polymers.* Sensors, 2008. **8**(1): p. 118-141.
31. Koev, S.T., et al., *Chitosan: an integrative biomaterial for lab-on-a-chip devices.* Lab Chip, 2010. **10**: p. 3026-3042.
32. Wu, L.Q., et al., *Mimicking biological phenol reaction cascades to confer mechanical function.* Adv Func Mat, 2006. **16**(15): p. 1967-1974.
33. Kim, E., et al., *Biomimetic approach to confer redox activity to thin chitosan films.* Adv Func Mat, 2010. **20**(16): p. 2683-2694.
34. Jara-Ulloa, P.A., S.E. Catalan-Caro, and C.A. Escobar, *Electrochemical characterizatio of new 1,5-benzodiazepine derivatives.* J of the Chilean Chem Soc, 2014. **59**(2): p. 2520-2522.
35. van Leeuwen, S.M., et al., *Prediction of clozapine metabolism by on-line electrochemistry/liquid chromatography/mass spectrometry.* Anal Bioanal Chem, 2005. **382**(3): p. 742-750.

36. Kauffmann, J.M., G.J. Patriarche, and G.D. Christian, *Electrochemical oxidation of derivatives of dibenzodiazepin, dibenzothiazepin and dibenzoxazepin.* Anal Lett, 1979. **12**(11): p. 1217-1234.
37. Arvand, M. and M.G. Shiraz, *Voltammetric determination of clozapine in pharmaceutical formulations and biological fluids using an in situ surfactant-modified carbon ionic liquid electrode.* Electroanalysis, 2012. **24**(3): p. 683-690.
38. Blankert, B., et al., *Horseradish peroxidase electrode for the analysis of clozapine.* Anal Lett, 2005. **37**(5): p. 903-913.
39. Farhadi, K. and A. Karimpour, *Electrochemical behavior and determination of clozapine on a glassy carbon electrode modified by electrochemical oxidation.* Analytical Sciences, 2007. **23**: p. 479-483.
40. Hammam, E., A. Tawfik, and M.M. Ghoneim, *Adsorptive stripping voltammetric quantification of the antipsychotic clozapine in bulk form, pharmaceutical formulation and human serum at a mercury electrode.* J Pharmaceut Biomed, 2004. **36**(1): p. 149-156.
41. Hernandez, L., E. Gonzalez, and P. Hernandez, *Determination of clozapine by adsorptive anodic voltammetry using glassy carbon and modified carbon paste electrodes.* Analyst, 1988. **113**(11): p. 1715-1718.
42. Huang, F., et al., *Sensitive detection of clozapine using a gold electrode modified with 16-mercaptohexadecanoic acid self-assembled monolayer.* Talanta, 2007. **72**(2): p. 457-462.
43. Mashhadizadeh, M.H. and E. Afshar, *Electrochemical investigation of clozapine at TiO2 nanoparticles modified carbon paste electrode and simultaneous adsorptive voltammetric determination of two antipsychotic drugs.* Electrochim Acta, 2013. **87**: p. 816-823.
44. Mohajeri, S.A., et al., *Clozapine recognition via molecularly imprinted polymers: Bulk polymerization versus precipitation method.* J Appl Polym Sci, 2011. **121**(6): p. 3590-3595.
45. Qu, S., et al., *Preparation of silicate nanotubes and its application for electrochemical sensing of clozapine.* Materials Letters, 2013. **102**: p. 56-58.
46. Shahrokhian, S., Z. Kamalzadeh, and A. Hamzehloei, *Electrochemical determination of clozapine on MWCNTs/New Coccine doped PPY modified GCE: an experimental design approach.* Bioelectrochem, 2013. **90**: p. 36-43.
47. Farhadi, K., et al., *Optimization of polymeric triiodide membrane electrode based on clozapine-triiodide ion-pair using experimental design.* Talanta, 2008. **76**(2): p. 320-326.
48. Al Attas, A.S., *Novel PVC membrane selective electrode for determinaton of clozapine in pharmaceutical preparations.* Int J Electrochem Sci, 2009. **4**: p. 9-19.
49. Albert, K.J., et al., *Cross-reactive chemical sensor arrays.* Chem Rev, 2000. **100**: p. 2595-2626.
50. Lavigne, J.J. and E.V. Anslyn, *Sensing a paradigm shift in the field of molecular recognition: from selective to differential responses.* Angew Chem Int Ed, 2001. **40**: p. 3118-3130.

51. Gardner, J.W. and P.N. Bartlett, *A brief history of electronic noses.* Sens Act B: Chem, 1994. **18**(1): p. 210-211.
52. Winquist, F., et al., *A hybrid electronic tongue.* Anal Chim Acta, 2000. **406**: p. 147-157.
53. Lvova, L., et al., *Electonic nose based on an array of metallic potentiometric sensors.* Talanta, 2006. **70**: p. 833-839.
54. Legin, A., et al., *Chemical sensor array for multicomponent analysis of biological liquids.* Anal Chim Acta, 1999. **385**: p. 131-135.
55. Winquist, F., P. Wide, and I. Lundstrom, *An electronic tongue based on voltammetry.* Anal Chim Acta, 1997. **357**: p. 21-31.
56. Gutes, A., et al., *Automatic sequential injection analysis electronic tongue with integrated reference electrode for the determination of ascorbic acid, uric acid and paracetamol.* Microchim Acta, 2007. **157**: p. 1-6.
57. Ivarsson, P., et al., *Discrimination of tea by means of voltammetric electronic tongue and different applied waveforms.* Sens Act B: Chem, 2001. **76**: p. 449-454.
58. Peres, A.M., et al., *An electronic tongue for gliadins semi-quantitative detection in foodstuffs.* Talanta, 2011. **83**: p. 857-864.
59. Bratov, A., N. Abramova, and A. Ipatov, *Recent trends in potentiometric sensor arrays- A review.* Anal Chem Acta, 2010. **67**(8): p. 149-159.
60. Verrelli, G., et al., *Development of silicon-based potentiometric sensors: Towards a miniaturized electronic nose.* Sens Act B: Chem, 2997. **123**: p. 191-197.
61. Gutierrez, M., S. Alegret, and M. del Valle, *Bioelectronic tongue for the simultaneous determination of urea, creatinine and alkaline ions in clinical samples.* Biosens and Bioel, 2008. **23**: p. 795-802.
62. Lvova, L., et al., *Multicomponent analysis of Korean green tea by means of disposable all-solid-state potentiometric electronic tongue microsystem.* Sens Act B: Chem, 2003. **95**: p. 391-399.
63. Ciosek, P., et al., *Analysis of dialysate fluids with the use of a potentiometric electronic tongue.* Microchim Acta, 2008. **163**: p. 139-145.
64. Hsueh, C.C., et al., *Chemically diverse modified electrodes: A new approach to the design and implementation of sensor arrays.* Anal Chim Acta, 1999. **397**: p. 135-144.
65. Kramer, R., *Chemometric techniques for quantitative analysis*. Vol. I. 1998: Marcel Dekker, Inc.
66. Vlasov, Y., et al., *Nonspecific sensor arrays (" electronic tongue") for chemical analysis of liquids (IUPAC Technical Report).* Pure Appl Chem, 2005. **77**(11): p. 1965-1983.
67. Scott, S.M., D. James, and Z. Ali, *Data analysis for electronic nose systems.* Microchim Acta, 2006. **156**(3-4): p. 183-207.
68. Ferraro, M.C., P.M. Castellano, and T.S. Kaufman, *A spectrophotometric-partial least squares (PLS-1) method for the simultaneous determination of furosemide and amiloride hydrochloride in pharmaceutical formulations.* J Pharmaceut Biomed, 2001. **26**(3): p. 443-451.

69. Ni, Y., Y. Wang, and S. Kokot, *Simultaneous determination of three fluoroquinolones by linear sweep stripping voltammetry with the aid of chemometrics.* Talanta, 2006. **69**(1): p. 216-225.
70. Reguera, C., M.C. Ortiz, and M.J. Arcos, *Differential pulse voltammetric simultaneous determination of four anti-inflammatory drugs by using soft modelling.* Electroanal, 2002. **14**(24): p. 1699-1706.
71. Rouhollahi, A., R. Rajabzadeh, and J. Ghasemi, *Simultaneous determination of dopamine and ascorbic acid by linear sweep voltammetry with chemometrics using a glassy carbon electrode.* Microchim Acta, 2007. **157**(3-4): p. 139-147.
72. Nevado, J.J., J.R. Flores, and G.C. Penalvo, *Simultaneous spectrophotometric determination of ethinylestradiol and levonorgestrel by partial least squares and principal component regression multivariate calibration.* Anal Chim Acta, 1997. **340**(1): p. 257-264.
73. Kim, E., et al., *Redox-cycling and H2O2 generation by fabricated catecholic films in the absence of enzymes.* Biomacromolecules, 2011. **12**: p. 880-888.
74. Ben-Yoav, H., et al., *A micro-system for clozapine antipsychotic treatment monitoring.* Biosens and Bioel, 2014. **(In preparation)**.
75. Ben-Yoav, H. and Chocron, S. E. et al. *The effect of vitamin C for point-of-care blood analysis applications using an electrochemical biosensor*. in *IEEE Sensors*. 2013. Baltimore, MD.
76. Ben-Yoav, H., et al., *A Whole Cell Electrochemical Biosensor for Water Genotoxicity Bio-Detection.* Electrochimica Acta, 2009. **54**(25): p. 6113-6118.
77. *Guideline EP07-A2: Interference Testing in Clinical Chemistry.* Clinical Laboratory Standards Institute (CLSI). 2002.
78. Psychogios, N., et al., *The human serum metabolome.* PloS one, 2011. **6**(2): p. e16957.
79. Krebs, H.A., *Chemical composition of blood plasma and serum.* Annu Rev Biochem, 1950. **19**(1): p. 409-430.
80. Palleschi, G., et al., *A study of interferences in glucose measurements in blood by hydrogen peroxide based glucose probes.* Anal Biochem, 1986. **159**(1): p. 114-121.
81. Raj, C.R. and T. Ohsaka, *Voltammetric detection of uric acid in the presence of ascorbic acid at a gold electrode modified with a self-assembled monolayer of heteroaromatic thiol.* J Electroanal Chem (Lausanne Switz), 2003. **540**: p. 69-77.
82. Mashhadizadeh, M.H. and E. Afshar, *Electrochemical investigation of clozapine at TiO2 nanoparticles modified carbon paste electrode and simultaneous adsorptive voltammetric determination of two antipsychotic drugs.* Electrochim Acta, 2013. **87**(816-823).
83. Wang, C., et al., *Differential pulse voltammetric determination of nimesulide in pharmaceutical formulation and human serum at glassy carbon electrode modified by cysteic acid/CNTs based on electrochemical oxidation of l-cysteine.* J Pharm Biomed Anal, 2006. **42**(2): p. 237-244.
84. Arai, K., et al., *Selective determination of chloride and bromide ions in serum by cyclic voltammetry.* Anal Biochem, 1996. **240**(1): p. 109-113.

85. Tonyushkina, K. and J.H. Nichols, *Glucose meters: a review of technical challenges to obtaining accurate results.* J Diabetes Sci Technol, 2009. **3**(4): p. 971-980.
86. Sanghavi, B.J., et al., *Nanomaterial-based electrochemical sensing of neurological drugs and neurotransmitters.* Microchim Acta, 2014: p. 1-41.
87. Netto, L.E.S., et al., *Reactive cysteine in proteins: protein folding, antioxidant defense, redox signaling and more.* Comp Biochem Physiol C Toxicol Pharmacol, 2007. **146**(1): p. 180-193.
88. Elias, J.R., D.J. McClements, and E.A. Decker, *Antioxidant activity of cysteine, tryptophan, and methionine residues in continuous phase β-lactoglobulin in oil-in-water emulsions.* J Agric Food Chem, 2005. **53**(26): p. 10248-10253.
89. Jones, D.P., et al., *Cysteine/cystine couple is a newly recognized node in the circuitry for biologic redox signaling and control.* FASEB J, 2004. **18**(11): p. 1246-1248.
90. Yao, J.K., R. Reddy, and D.P. van Kammen, *Reduced level of plasma antioxidant uric acid in schizophrenia.* Psychiatry Res, 1998. **80**(1): p. 29-39.
91. Monk, P., *Fundamentals of Electro-Analytical Chemistry*2001: John Wiley & Sons Ltd.
92. Kamau, G.N., *Surface preparation of glassy carbon electrodes.* Anal Chim Acta, 1988. **207**: p. 1-16.
93. Chen, P. and R.L. McCreery, *Control of electron transfer kinetics at glassy carbon electrodes by specific surface modification.* Anal Chem, 1996. **68**(22): p. 3958-3965.
94. Lu, M. and R.G. Compton, *Voltammetric pH sensing using carbon electrodes: glassy carbon behaves similarly to EPPG.* Analyst, 2014.
95. Wang, C., et al., *Covalent modification of glassy carbon electrode with L-cysteine for the determination of acetaminophen.* Microchim Acta, 2006. **155**(3-4): p. 365-371.
96. Deinhammer, R.S., et al., *Electrochemical oxidation of amine-containing compounds: a route to the surface modification of glassy carbon electrodes.* Langmuir, 1994. **10**(4): p. 1306-1313.
97. O'Neill, R.D., et al., *Comparisons of platinum, gold, palladium and glassy carbon as electrode materials in the design of biosensors for glutamate.* Biosens Bioelectron, 2004. **19**(11): p. 1521-1528.
98. Conway, B.E., *Electrochemical oxide film formation at noble metals as a surface-chemical process.* Prog Surf Sci, 1995. **49**(4): p. 331-452.
99. Gutes, A., et al., *Automatic sequential injection analysis electronic tongue with integrated reference electrode for the determination of ascorbic acid, uric acid and paracetamol.* Microchim Acta, 2007. **157**(1-2): p. 1-6.
100. Zhou, M., et al., *Electrochemical Behavior of L-Cysteine and Its Detection at Ordered Mesoporous Carbon-Modified Glassy Carbon Electrode.* Anal Chem, 2007. **79**(14): p. 5328-5335.
101. Spataru, N., et al., *Voltammetric determination of L-cysteine at conductive diamond electrodes.* Anal Chem, 2001. **73**(3): p. 514-519.

102. Grootveld, M. and B. Halliwell, *Measurement of allantoin and uric acid in human body fluids. A potential index of free-radical reactions in vivo?* Biochem J, 1987. **243**: p. 803-808.
103. Dhariwal, K.R., W.O. Hartzell, and M. Levine, *Ascorbic acid and dehydroascorbic acid measurements in human plasma and serum.* Am J Clin Nutr, 1991. **54**(4): p. 712-716.
104. Gutierrez, M., S. Alegret, and M. del Valle, *Bioelectronic tongue for the simultaneous determination of urea, creatinine and alkaline ions in clinical samples.* Biosens Bioelectron, 2008. **23**(6): p. 795-802.
105. Gutes, A., et al., *Automatic sequential injection analysis electronic tongue with integrated reference electrode for the determination of ascorbic acid, uric acid and paracetamol.* Microchim Acta, 2007. **157**(1-2): p. 1-6.
106. Albert, K.J., et al., *Cross-reactive sensor arrays.* Chem Rev, 2000. **100**(7): p. 25995-2626.
107. Lavigne, J.J. and E.V. Anslyn, *Sensing a paradigm shift in the field of molecular recognition: From selective to differential receptors.* Angew Chem Int Ed Engl, 2001. **40**(17): p. 3118-3130.
108. Oertel-Knochel, V., et al., *Discovery and development of integrative biological markers for schizophrenia.* Prog Neurobiol, 2011. **95**(4): p. 686-702.